

UNIVERSITY OF MODENA AND REGGIO EMILIA
Department of Engineering “Enzo Ferrari”

Master Degree Course in Civil Engineering (D.M. 270/04)

Optimizing Tied-Arch Bridges for Sustainability: A Study on Arch Size and Shape Modification

FILIPPO RIBES

Supervisor:
Prof. Bruno Briseghella

Co-Supervisor:
Ing. Elisa Bassoli

ACADEMIC YEAR 2022/2023

Abstract

In a world focused on environmental sustainability, optimizing the design of road bridges not only brings economic advantages but also plays a crucial role in promoting a greener and more environmentally conscious future. Utilizing optimization algorithms and parametric designs is a pivotal key in achieving this objective, allowing us to design infrastructures that are both sustainable and resilient, especially those characterized by a significant amount of carbon dioxide emissions (CO_2) like bridges. To address this need, we developed an optimization algorithm that assesses the environmental impact of tied-arch bridges, a common infrastructure type worldwide. Our algorithm focuses on the arch's geometry, particularly its shape and cross-sections, and it is tailored to road bridges made of steel that are straight and have a deck with constant length and width. To evaluate our system, we studied an existing tied-arch bridge and its arch's steel usage, cost and CO_2 equivalent emissions. In order to formulate an optimization plan, these metrics were then compared with those of five different variations of the same bridge with altered parameters generated with the algorithm. The results of the studied variants confirm the actual design quality of the analyzed bridge, but suggest a non-negligible potential for carbon dioxide reduction of up to 6.80 %.

Keywords: Structural Optimization, Tied-Arch Bridges, Sustainability, Computational-based Optimization, Parametrization

Acknowledgements

I would like to express my deepest gratitude to my thesis supervisor, professor Bruno Briseghella, for his unwavering support, invaluable guidance, and immense expertise throughout the entire research process. His dedication to excellence and passion for the subject matter have been, becoming a source of inspiration for me.

I am also grateful to my co-supervisor, engineer Elisa Bassoli, whose insightful feedback and constructive criticism have significantly contributed to the refinement of this work. Her commitment to academic excellence and her willingness to share her knowledge have been instrumental in shaping the outcome of this thesis.

Ringrazio in particolare mia madre e mio padre per avermi sostenuto e supportato, sia economicamente che emotivamente, nell'intero percorso di studi ed avermi permesso di essere quello che sono ora. Un immenso ringraziamento va poi a mio fratello Ste, che non si è mai tirato indietro nel sacrificare tempo ed energie per ascoltarmi, dispensandomi sempre consigli dall'estrema utilità. Ringrazio anche i miei cugini Anton e Rubes e le mie zie Lena e Isola che, tra una telefonata e l'altro, hanno saputo arricchire i miei momenti di studio e di vita quotidiana, mostrandomi il loro affetto.

Ci tengo poi a ringraziare il mio amico Endriu che, sebbene i chilometri che ci separano, è tra le persone che più è stata presente quando avevo davvero bisogno, non facendomi sentire mai solo.

Come potrei poi non ringraziare il buon Sandro, una delle persone più sagge che abbia mai incontrato. Tra una lezione di water ed uno specialino al bar, abbiamo legato subito, anche se ci conosciamo da appena un anno.

Un affettuoso ringraziamento va poi a te Vale: il nostro legame è un continuo caleidoscopio di emozioni e di sentimenti, maturato negli anni e mai rimasto invariato, tra momenti di amore e odio reciproco, ma sempre legato da quel filo rosso invisibile che ci unisce, e che ancora non sapremo dove ci porterà.

Vorrei infine ringraziare il team della *Giancarlo Maselli S.r.l Diagnostica & Engineering* per avermi offerto la possibilità di intraprendere un'interessantissima esperienza lavorativa. Nello specifico, ringrazio il professor Giancarlo Maselli, che ha creduto in me offrendomi quest'opportunità di lavoro e trattandomi sempre con forte riguardo e affetto, permettendomi di pagarmi da solo buona parte degli studi e donandomi la tanto agognata indipendenza economica. Vuoi anche forse per la forte somiglianza estetica verso mio padre, è stato e continuerà ad essere come un nonno per me, quel nonno che non ho mai avuto.

A tutti voi un sentito grazie.

Filippo, Correggio, 5/12/2023

Contents

List of Figures	ix
List of Tables	xi
1 Introduction	1
2 Background	3
2.1 The Optimization Process	3
2.1.1 Objective Function	4
2.1.2 Search Space	4
2.1.3 Constraints	5
2.2 Optimization in Structural Design	6
2.3 Tied-Arch Bridges and Box Girders Properties	7
2.4 Influence Lines	7
2.5 Resistance of Tied-Arch Bridges	8
2.5.1 Elastic and Plastic Section Modulus	10
2.6 Stability of Tied-Arch Bridges	11
2.6.1 Directional Stability and Snap-Through Analysis	13
2.6.2 Lateral Stability	16
2.6.3 First-Order and Second-Order Analysis	17
2.7 Carbon Dioxide Emissions in Steel Production	19
3 Methods	21
3.1 Case Study of an Existing Tied-Arch Bridge: Bridge over the Carpi's Highway Station	21
3.2 Modeling the Optimization Problem	22
3.2.1 Design Variables	22
3.2.2 Dependent Variables	23
3.2.3 Preassigned Parameters	26
3.2.4 Objective Function	26
3.2.5 Constraints	27
3.3 Parametric Shape Modeling and Sizing Cross-Sections of the Arch . .	27
3.3.1 Arch Shape Parametrization	27
3.3.2 Arch Shape for the Second-Order Analysis	29
3.3.3 Arch Cross-Sections Parametrization	30
3.4 Finite Element Model (FEM)	31

3.4.1	FEM Modeling	32
3.4.2	Acting Loads	33
3.4.3	FEM Solvers	33
3.5	Stability Analyses	34
3.6	Python Development	34
3.6.1	Constants, Dependent Variables and Design Variables	35
3.6.2	Functions Definition	35
3.6.3	Python Constraints	36
3.6.4	Reporting of the Results	36
4	Results and Discussion	39
4.1	Objective Function Results for the Reference Design	39
4.2	Proposed Conceptual Designs	39
4.2.1	Common Structural Aspects	40
4.2.2	Conceptual Design 1: A Rise-to-Span Ratio of 0.03	42
4.2.3	Conceptual Design 2: A Rise-to-Span Ratio of 0.06	43
4.2.4	Conceptual Design 3: A Rise-to-Span Ratio of 0.09	43
4.2.5	Conceptual Design 4: A Rise-to-Span Ratio of 0.12	46
4.2.6	Conceptual Design 5: A Rise-to-Span Ratio of 0.15	46
4.3	Discussion	50
5	Conclusion	53
5.1	Future Work	53
5.1.1	API Implementation	53
5.1.2	SciPy Optimization in Python	53
5.1.3	Increase Level of Design Detail	54
5.1.4	Multi Objective Optimization	54
	Bibliography	55

List of Figures

2.1	(a) Suspension bridge	8
2.2	(b) Arch bridge	8
2.3	(c) Tied-arch bridge	8
2.4	<i>Some examples of suspension bridge, arch bridge and tied-arch bridge [29]–[31].</i>	8
2.5	<i>Influence line and principle of Maxwell’s reciprocal theorem [26]–[28].</i>	9
2.6	<i>An example of deformation and stress diagram representation at the elastic limit for bending around the x-axis [33].</i>	11
2.7	<i>An example of the complete plasticization of the section by bending around the x-axis [33].</i>	11
2.8	<i>Buckling curves, as reported in EN 1993-1 (2005) - “Buckling resistance of Members” [33].</i>	13
2.9	<i>Imperfection factor α for buckling curves, as reported in Table 6.1 of EN 1993-1 (2005) - “Buckling resistance of Members” [33].</i>	13
2.10	<i>Selection of buckling curve for a cross-section, as reported in Table 6.2 of EN 1993-1 (2005) - “Buckling resistance of Members” [33]. . .</i>	14
2.11	<i>In-plane buckling factor β, as shown in EN 1993-2 (2006), Annex D.3 - “Arches Bridges” [35].</i>	15
2.12	<i>Snap-through stable states of a generic elastic arch under a downward force F gradually applied to its apex [36].</i>	16
2.13	<i>The snap-through dimensionless K factor, as shown in Table D.5 of EN 1993-2 (2006), Annex D.3 - “Arches Bridges” [35].</i>	16
2.14	<i>Out-of-plane buckling factor β_1, as shown in Table D.6 of EN 1993-2 (2006), Annex D.3 - “Arches Bridges” [35].</i>	17
2.15	<i>Out-of-plane buckling factor β_2, as shown in Table D.7 of EN 1993-2 (2006), Annex D.3 - “Arches Bridges” [35].</i>	17
2.16	<i>Imperfections for in-plane buckling of arches, as shown in Table D.8 of EN 1993-2 (2006), Annex D.3 - “Arches Bridges” [35].</i>	18
2.17	<i>Imperfections for out-of-plane buckling of arches, as shown in Table D.9 of EN 1993-2 (2006), Annex D.3 - “Arches Bridges” [35].</i>	18
3.1	<i>Elevation showing the original design of the bridge over the Carpi’s highway station, longitudinal profile and deck plan respectively.</i>	22
3.2	<i>Elevation showing the original design of the bridge over the Carpi’s highway station, transversal section.</i>	23

3.3	<i>Elevation showing the original design of the arch's cross-section of the bridge over the Carpi's highway station. The section is constant along its entire development.</i>	23
3.4	<i>Summarized flowchart diagram of the optimization problem.</i>	24
3.5	<i>Geometry-dependent variables.</i>	24
3.6	<i>Flowchart diagram of the parametrization step.</i>	27
3.7	<i>Arch shape parametrization. A function is assigned to each z-coordinate instead a fixed value.</i>	28
3.8	<i>Second-order arch shape parametrization, transversal view.</i>	30
3.9	(a) Initial reference design	30
3.10	(b) Final design	30
3.11	<i>Reference and final design of arch's cross-section.</i>	30
3.12	<i>If-else statement of the FEM step.</i>	32
3.13	<i>For-loop of the stability analyses step.</i>	34
3.14	<i>For-loop of the Python implementation step.</i>	35
3.15	<i>Flowchart diagram of the optimization problem.</i>	37
4.1	<i>Elevation showing the box girder section of the reference bridge over the Carpi's Highway Station, including their geometries expressed in millimeters. We decided to leave the deck shape unchanged.</i>	40
4.2	<i>Oversize transient load applied across the deck of the bridge. Distances are expressed in meters and the forces in kN.</i>	41
4.3	<i>Finite element model for conceptual design 1, having a rise-to-span ratio of 0.03.</i>	42
4.4	<i>Finite element model for conceptual design 2, having a rise-to-span ratio of 0.06.</i>	43
4.5	<i>Finite element model for conceptual design 3, having a rise-to-span ratio of 0.09.</i>	43
4.6	<i>Finite element model for conceptual design 4, having a rise-to-span ratio of 0.12.</i>	46
4.7	<i>Finite element model for conceptual design 5, having a rise-to-span ratio of 0.15.</i>	46
4.8	<i>Arch area saving and the objective function scores percentage for each conceptual design (C.D.) compared to the original design.</i>	51

List of Tables

3.1	<i>Dependent variables with their reference units.</i>	25
3.2	<i>Preassigned parameters which the user can override with their default values and units.</i>	26
3.3	<i>Parameters used for the parametrization of the arch cross-section, including their acronyms and units.</i>	31
4.1	<i>Arch cross-sectional area (A_a) and objective function results (steel weight $W_{tot,a}$, cost $C_{tot,a}$ and carbon dioxide emitted $CO_{2eqe,a}$) for the reference design (R.D).</i>	39
4.2	<i>Non-structural dead loads, including their values and units.</i>	41
4.3	<i>Geometries, parameters, stresses and final objective function results for conceptual design 1, having a rise-to-span ratio of 0.03.</i>	44
4.4	<i>Geometries, parameters, stresses and final objective function results for conceptual design 2, having a rise-to-span ratio of 0.06.</i>	45
4.5	<i>Geometries, parameters, stresses and final objective function results for conceptual design 3, having a rise-to-span ratio of 0.09.</i>	47
4.6	<i>Geometries, parameters, stresses and final objective function results for conceptual design 4, having a rise-to-span ratio of 0.12.</i>	48
4.7	<i>Geometries, parameters, stresses and final objective function results for conceptual design 5, having a rise-to-span ratio of 0.15.</i>	49
4.8	<i>Arch cross-sectional area (A_a) and objective function results (steel weight $W_{tot,a}$, cost $C_{tot,a}$ and carbon dioxide emitted $CO_{2eqe,a}$) for both the reference design (R.D) and each conceptual design studied (C.D).</i>	51
4.9	<i>Objective function scores (steel weight W_{score}, cost C_{score} and carbon dioxide emitted $CO_{2eqe,score}$) calculated for each conceptual design, along with their percentage difference compared to the original design.</i>	51

1

Introduction

In a continuously evolving world, the field of civil engineering plays an increasingly fundamental role in a nation's development. The need to create sustainable and resilient infrastructure, capable of minimizing environmental degradation and preserving natural resources for future generations, has become an absolute priority. In fact, Long *et al.* [1] affirm that the impact of global emissions and climate change is significantly influenced by urban centers worldwide, encompassing only 2 % of the Earth's surface yet contributing to nearly 80 % of carbon emissions from human activities. The urban setting directly shapes our living standards, social welfare, and health. Therefore, the attributes and excellence of our infrastructures play a pivotal role in favoring urban sustainability and the overall health of our surroundings, considering that they constitutes at least 50 % of our national wealth [1]. In this context, parametric designs and optimization algorithms emerge as essential tools for guiding the decision-making process in civil engineering, enabling the planning of efficient and environmentally responsible solutions. Hence, extensive research and practical applications of new materials, construction methods, and design techniques are necessary [2].

This thesis focuses on modern optimization algorithms and parametric designs to evaluate the environmental impact of tied-arch bridges (a common infrastructure type worldwide). The focus is directed towards the arch's shape and geometries with the aim of reducing steel requirements, consequently lowering costs and carbon dioxide emissions. To achieve this objective, a real tied-arch bridge was analyzed to validate the algorithm. This first chapter serves as an introduction to the topic.

The second chapter begins with an introduction to the fundamental concepts of the optimization process, guiding the reader to the subsequent discussion on structural optimization. It further delves into the properties of tied-arch bridges and influence lines. Finally, the chapter addresses the analyses conducted on them in accordance with the Eurocodes, followed by the definition of the Global Warming Potential (GWP) [3], [4].

In the third chapter, an extensive exploration of the algorithm is given. This includes an in-depth look at the modeling of the optimization problem, the process of sizing and modeling the arch, the development of a finite element model (FEM), and the management of constraints. This chapter is the most comprehensive, and great care and attention were given to its content.

The algorithm was assessed by utilizing it to optimize an existing tied-arch bridge by comparing it to five alternative design scenarios. The methodology and results of these case studies are detailed in the fourth chapter.

The fifth and final chapter of the thesis concludes by examining the degree to which the intended goals have been achieved. Additionally, it offers suggestions into potential areas for future research within this field.

2

Background

Numerical optimization methods serve as powerful tools that allow to uncover solutions that maximize efficiency, minimize material usage, or achieve desired outcomes and this can be exploited very well in civil engineering problems [2], [5]–[7]. Most traditional optimization algorithms are deterministic [5]. To address the intricacies of numerous real-world optimization challenges, many turn to metaheuristic algorithms, which draw inspiration from stochastic natural phenomena through the integration of randomization [8]–[10]. However, due to the limited availability of information and instrumentation, this thesis will address a manual optimization approach [11].

The chapter begins by presenting the fundamental theory of numerical optimization, followed by the problem of carbon dioxide emissions in steel production industry. Then, the optimization in structural design are discussed, and influence lines are introduced. We focus on handling resistance and buckling analyses for tied-arch bridges, concluding with the definition of the Global Warming Potential [3], [4].

2.1 The Optimization Process

The conventional process of optimization involves modifying the input of a function or procedure with the aim of either diminishing or augmenting the resulting output value [2], [5], [6]. The function under consideration for optimization is commonly referred to as the *objective function* and an array of input values constitutes a *solution*. Additionally, constraints are typically imposed, delimiting the permissible range of input values. A solution that satisfies constraints is called a *feasible solution*, and the collection of allowable input values defines the *search space*. Consequently, the search space delineates the domain encompassing all feasible solutions. Mathematically, the formulation of an optimization problem¹ is as follows:

$$\text{minimize } f_i(\mathbf{x}), \quad i = 1, 2, \dots, M \quad (2.1)$$

subject to the constraints:

¹This can be a minimization but also a maximization.

$$\begin{aligned} g_j(\mathbf{x}) &\leq 0, \quad j = 1, 2, \dots, J \\ h_k(\mathbf{x}) &= 0, \quad k = 1, 2, \dots, K \end{aligned} \tag{2.2}$$

where $f_i(\mathbf{x})$, $g_j(\mathbf{x})$ and $h_k(\mathbf{x})$ are functions of the *design vector*:

$$\mathbf{x} = (x_1, x_2, \dots, x_D), \quad \mathbf{x} \in \mathbb{R}^D \tag{2.3}$$

The components x_i of the design vector are called *design variables*, the functions $f_i(\mathbf{x})$ are the objective functions, and the inequalities $g_j(\mathbf{x})$ and equalities $h_k(\mathbf{x})$ are the constraints.

An optimization problem can have an arbitrary number of objective functions. The optimization process is classified as *single-objective optimization* if there is only one objective function, and as *multi-objective optimization* if there are more than one objective function. Therefore, a single-objective optimization has the aim to find a single optimal solution, while multi-objective optimization seeks to find a set of solutions instead. These solutions are known as the Pareto front [2], [5], where no solution is better than another in all objectives [12].

2.1.1 Objective Function

The objective function is a numerical representation of the process that we are seeking optimal input values to [2], [5], [6]. Thus, the output of the objective function is the quantity to be optimized. For example, if the purpose is to minimize the environmental impact of a bridge construction by reducing the amount of its CO₂ (the carbon dioxide) equivalent, the output of the objective function should be the CO₂ equivalent emitted. The input to the function are the design variables. All other parameters necessary to determine the CO₂ equivalent emitted is provided as constants (or functions of the design variables) within the objective function.

2.1.2 Search Space

The number of design variables determines the *dimensionality* of the optimization problem, where n variables correspond to an n -dimensional problem [2], [5]. A simple problem with only two design variables can be visualized in a comprehensible manner with a surface plot, usually called *landscape*. In such a plot, each pair of x and y coordinates represents a point in the search space, and the corresponding z -coordinate represents the value of the objective function at that particular point. Typically, objective functions have several *local optima*, but only one *global optimum*. What is referred to as optimum depends on whether we are seeking a minimum or a maximum of the function. By convention, it is assumed that the objective function should be minimized. If the objective function should be maximized instead, we can simply invert the sign of the function and minimize.

2.1.3 Constraints

Constraints refer to the limitations, conditions, or requirements that guide the process of improving an algorithm [2], [5], [6]. These constraints can encompass various aspects, such as time, accuracy and compatibility. In this way, constraints set the boundaries and expectations for the optimization process, ensuring that the algorithm aligns with specific criteria or limitations. For this reason, optimization problems can be classified according to the constraints: a problem without constraints is an *unconstrained optimization problem* and a problem with constraints is a *constrained optimization problem* [5]. While many optimization algorithms are most effective when dealing with unconstrained variables, real-world problems often involve constraints. The basic idea of constraint-handling techniques is to transform a constrained optimization problem into an unconstrained one [13]. An example of this is the penalty method [14]. Constraints can fall into two primary categories: *linear* and *non-linear* [15]–[17]. Linear constraints are relatively easy to manage since they delineate infeasible regions and narrow down the search space directly. They can be evaluated without the need of computationally intensive operations. In contrast, non-linear constraints make the optimization problem more challenging to solve. In this thesis we focus on *penalty method* [14] to handle non-linear constraints.

The penalty method is a widely efficient approach thanks to its fundamental principle which involves assigning a penalty value to a solution that fails to satisfy the constraints. This penalty value is then added to the objective function, forming the *penalized objective function* [5], which can be formulated as:

$$\Pi(\mathbf{x}, \boldsymbol{\mu}, \boldsymbol{\nu}) = f(\mathbf{x}) + P(\mathbf{x}, \boldsymbol{\mu}, \boldsymbol{\nu}) \quad (2.4)$$

where $f(\mathbf{x})$ is the objective function and $P(\mathbf{x}, \boldsymbol{\mu}, \boldsymbol{\nu})$ is the *penalty term*. The penalty term has several popular definitions, one of them can be defined as:

$$P(\mathbf{x}, \boldsymbol{\mu}, \boldsymbol{\nu}) = \sum_{j=1}^J \mu_j \max(0, g_j(\mathbf{x}))^2 + \sum_{k=1}^K \nu_k |h_k(\mathbf{x})|, \quad (2.5)$$

where $\mu_j > 0$ and $\nu_k > 0$ are the *penalty factors*. Another popular definition of the penalty term is:

$$P(\mathbf{x}, \boldsymbol{\mu}, \boldsymbol{\nu}) = \sum_{j=1}^J \mu_j H_j [g_j(\mathbf{x})] g_j^2(\mathbf{x}) + \sum_{k=1}^K \nu_k H_k [h_k(\mathbf{x})] h_k^2(\mathbf{x}), \quad (2.6)$$

where $\mu_j > 0$ and $\nu_k \gg 1$. The factors $H_j[g_j(\mathbf{x})]$ and $H_k[h_k(\mathbf{x})]$ fulfill the conditions:

$$H_j[g_j(\mathbf{x})] = \begin{cases} 0 & \text{if } g_j(\mathbf{x}) \leq 0, \\ 1 & \text{otherwise,} \end{cases}$$

$$H_k[h_k(\mathbf{x})] = \begin{cases} 0 & \text{if } h_k(\mathbf{x}) = 0, \\ 1 & \text{otherwise.} \end{cases}$$

To simplify the implementation, it is also possible to consider $\mu = \mu_j$ for all j and $\nu = \nu_k$ for all k . In this case, the penalized objective function of the Equation 2.4 can be written as:

$$\Pi(\mathbf{x}, \boldsymbol{\mu}, \boldsymbol{\nu}) = f(\mathbf{x}) + \mu \sum_{j=1}^J H_j [g_j(\mathbf{x})] g_j^2(\mathbf{x}) + \nu \sum_{k=1}^K H_k [h_k(\mathbf{x})] h_k^2(\mathbf{x}). \quad (2.7)$$

In Equation 2.7, it is clear that the penalty term is directly proportional to the magnitude of the constraint violations. This relationship is evident because significant violations of the constraints should result in a substantial penalty within the objective function. This penalty serves to guide the algorithm away from regions in the search space where feasibility is compromised. In a manual approach, however, it alerts us whether the path we are following will actually lead to optimization or not.

2.2 Optimization in Structural Design

A structure to be optimized can be defined through a collection of quantities, which can be categorized into two different type of values [2], [5], [6]:

- *Preassigned parameters*;
- *Variables*;

Preassigned parameters maintain a constant value throughout the optimization process. Their optimal values are not fixed, but are necessary for defining the computational structure. Conversely, variables are changeable quantities that can be further divided into two categories [5], [6], [18], [19]:

- *Independent variables*: these are the focus of optimization algorithms, and their optimal values are adjusted or varied to enhance the performance or efficiency of a given structure;
- *Dependent variables*: these variables are influenced by the choices made for the independent variables and represent the desired optimal outcomes.

In particular, independent variables are also known as *design variables* and they can be adjusted or modified within certain predefined bounds or constraints to find the best solution to our problem [20]. Because of that, they are the main focus of our study. Dependent variables, on the other hand, encompass all quantities that are neither independent variables nor preassigned parameters.

The decision to treat a quantity in a structure design as a design variable, a dependent variable or preassigned parameter requires thoughtful consideration, guided by several key inquiries [5]:

- How does a variation in the quantity impact the objective?
- Are there challenging-to-quantify constraints, such as aesthetics?
- Is the parameter value open for the designer's choice, or is it predetermined?

- Is there experiential knowledge suggesting a particular parameter value yields favorable results?

In many cases, the optimization task can be simplified by assuming fixed values for most quantities and concentrating optimization efforts on a subset of design variables. This consideration should influence the definition of the optimization problem, focusing on quantities that significantly influence outcomes.

Design variables can be categorized based on the property of the structure they represent, typically falling into four groups [2], [5], [6]:

- Material properties;
- Structural system topology (interconnections of members);
- Structural system geometry (shape);
- Cross-sectional dimensions (size) of structural members.

Optimizing the topology, shape, or size of a structural system is generally more suitable for reducing weight and, therefore, cost and CO₂ emissions than optimizing material properties [5]. Additionally, material properties are frequently chosen from a discrete set of manufacturing standards, increasing the problem complexity. Therefore, material parameters are frequently treated as preassigned parameters [5].

2.3 Tied-Arch Bridges and Box Girders Properties

A tied-arch bridge combines features from both suspension and arch bridges. Unlike traditional arch bridges, the arch is positioned above the deck, and vertical cables are attached to it, supporting the deck as shown in Figure 2.4. These vertical cables work in tension and compression to distribute the load [21]–[23]. Furthermore, many arch bridges employ box girders, which take on the function of the deck [24], [25]. A box girder is a type of enclosed tube beam with multiple walls, resembling a box or hollow rectangle. Box girders are widely used due to their exceptional structural efficiency and versatility. They offer high torsional stiffness, ensuring balanced load distribution from side to side, and a high moment of inertia relative to their weight, allowing them to carry heavy loads with minimal material usage.

In terms of managing vertical loads, a tied-arch bridge can be compared to a *compressed arch-tensioned deck system*, with the torsional moment managed by the box girder. An advantageous feature of this bridge design is its independence from horizontal compression forces for structural integrity. This characteristic allows for off-site construction, followed by transportation and installation.

2.4 Influence Lines

To study how loads are distributed throughout the bridge’s structure, influence lines stand as valuable tools. They are graphical representations used for analyzing the impact of moving loads, such as vehicles or other dynamic forces, on specific structural



(a) Suspension bridge

(b) Arch bridge

(c) Tied-arch bridge

Figure 2.4: *Some examples of suspension bridge, arch bridge and tied-arch bridge [29]–[31].*

elements [26], [27]. These representations consider the dynamic effects induced by moving loads. As the load traverses the structure, it can trigger oscillations and dynamic responses, which influence lines help quantify. These lines play a pivotal role in the design and assessment of structures, particularly those exposed to dynamic loads like bridges.

The purpose of influence lines is to determine the worst-case scenario for the impact of a moving load on a structural element. The horizontal axis of the influence line represents the position of the moving load, and the vertical axis represents the corresponding response. By plotting these lines, the location along the structure where the dynamic load produces the maximum effect can be found. Taking for example the simply supported beam in Figure 2.5, the influence line for the bending moment in section S given by a moving load F returns the diagram on the right side of the figure: when the force F is located in section A or section B , the value of the bending moment in section S is 0; when it is located in section S , the maximum bending moment for the section S is reached.

The theory behind the influence lines is given by the principal of Maxwell’s reciprocal theorem [28], which states that, for two identical forces at points B and A on a linear elastic structure as shown in Figure 2.5, the displacement at A caused by a unit force at B is the same as the displacement at B caused by a unit force at A.

2.5 Resistance of Tied-Arch Bridges

Resistance analysis is essential for evaluating a bridge’s ability to withstand various loads and forces [23], [32]. It ensures safety, structural integrity, and compliance with standards. Resistance analysis complements influence lines, which help identify critical load points and stress distributions within the bridge, and it is particularly decisive for *Ultimate Limit States* (ULS) [33], [34], referring to the most severe loading scenarios that structures must withstand without compromising safety and performance throughout their service life. These states represent conditions in which a structure is at risk of failure, and they are defined by the resistance of cross-sections

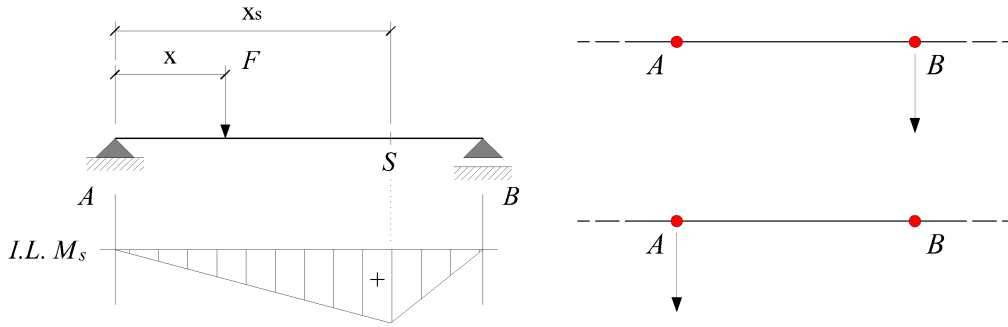


Figure 2.5: *Influence line and principle of Maxwell's reciprocal theorem [26]–[28].*

and members based on tests in which the material exhibited sufficient ductility to apply simplified design models.

By considering tied-arch bridges, they involve various structural elements like the deck, the hangers, the abutments and the arch itself. In particular, according to the EN 1993-1-1 (2005), Section 6.2: “Resistance of cross sections” [33], the design value of an action effect in each cross-section shall not exceed the corresponding design resistance, so tension or compression, shear stress and bending moment acting on the structure must be verified. Furthermore, the design values of resistance should depend on the classification of the cross-section.

In general, the design resistance R_d is given by:

$$R_d = \frac{R_k}{\gamma_M} \quad (2.8)$$

where R_k is the characteristic value of the resistance (tension, compression, shear stress or bending moment) of the member and γ_M is the recommended partial factor. R_k is determined by the characteristic values of the resistance of the f_{yk} materials and by the geometric characteristics of the structural elements, dependent on the class of the section. Based on the stress to be verified, the following conditions must be satisfied:

$$N_{Ed}, V_{Ed}, M_{Ed} \leq R_d \quad (2.9)$$

Where N_{Ed} is the tension or compression stress, V_{Ed} is the shear stress, and M_{Ed} is the bending moment stress.

For *tension* or *compression*, the design value of the tension or compression force N_{Ed} at each cross-section shall satisfy:

$$N_{Ed} \leq N_{Rd} = \frac{f_{yk}}{\gamma_M} \cdot A \quad (2.10)$$

where N_{Rd} is the design tension or compression resistance, f_{yk} is the nominal values of the characteristic yield strength and A is the cross-sectional area.

For *shear stress*, the design value of the shear stress force V_{Ed} at each cross section shall satisfy:

$$V_{Ed} \leq V_{Rd} = \frac{f_{yk}}{\gamma_M \cdot \sqrt{3}} \cdot A \quad (2.11)$$

where V_{Rd} is the design shear stress resistance.

For *bending moment*, the design value of the bending moment M_{Ed} at each cross-section shall satisfy:

$$M_{Ed} \leq M_{Rd} = \frac{f_{yk}}{\gamma_M} \cdot W_{x,y} \quad (2.12)$$

where M_{Rd} is the design bending moment resistance and $W_{x,y}$ is the section modulus, which is a geometric property of the section and it can be calculated about the two principal axes of inertia x and y .

An in-depth study of the resistance modulus proposed in the following subsection is necessary to understand how it is used in this analysis.

2.5.1 Elastic and Plastic Section Modulus

As previously explained, the section modulus $W_{x,y}$ is a geometric property of the section used to determine the design bending moment resistance of the cross-section [33]. Specifically, it is further divided into two parts, obtained by considering the elastic (W_{el}) or plastic (W_{pl}) field of the steel cross-section.

The elastic section modulus represents a cross-section's resistance to bending without causing plastic deformation of the material. It is defined within the elastic range, where the extreme fibers of the section in compression or tension reach the yield stress of the steel. This can be calculated about the x and y axes, respectively, as:

$$W_{el,x} = \frac{I_x}{y_{max}} \quad (2.13)$$

$$W_{el,y} = \frac{I_y}{x_{max}} \quad (2.14)$$

where y_{max} and x_{max} are the distances of the furthest fiber from y and x axes respectively. An example representation is shown in the Figure 2.6.

The plastic section modulus assesses a cross-section's resistance to bending, allowing for plastic deformation without failure. It is calculated based on the full cross-sectional area, as shown in Figure 2.7, and depends on the first moment of inertia².

²The first moment of inertia is used to measure the distribution of an area relative to an axis.

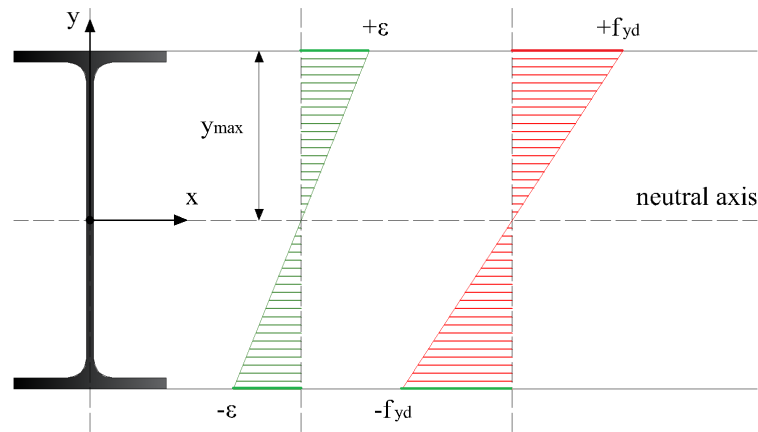


Figure 2.6: An example of deformation and stress diagram representation at the elastic limit for bending around the x -axis [33].

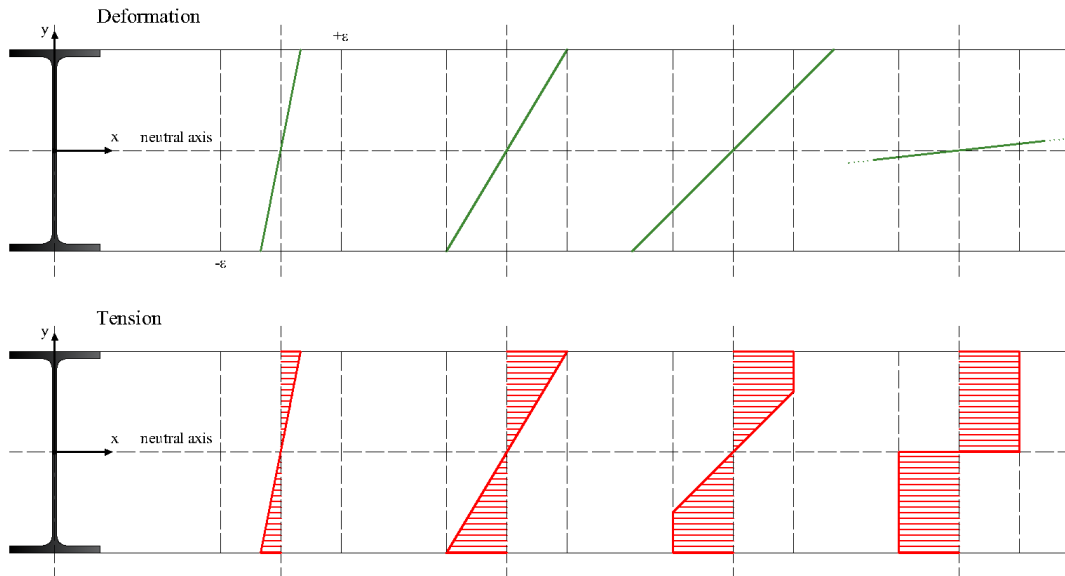


Figure 2.7: An example of the complete plasticization of the section by bending around the x -axis [33].

The choice of which module to use for the calculation depends on the section type, classified according to Eurocodes into classes 1, 2, 3, or 4 and they vary in terms of the rotational capacity of the sections. Further information can be found in EN 1993-1 (2005), Section 5.5: “Classification of Cross-Sections” [33].

2.6 Stability of Tied-Arch Bridges

In addition to the resistance analysis, a pressure-bent elements analysis must be carried out, when relevant, including the *Eulerian buckling analysis* [21]. In fact, when a structure is subjected to specific external loads, its state of equilibrium can

experience a significant and potentially dangerous displacement if these loads surpass a critical level and increase even slightly beyond that point. This critical load level is typically referred to as the *buckling state* and the associated load is known as the *critical buckling load*.

Regarding the arch of a tied-arch bridge, two different types of analysis must be conducted [21], and they will be discussed in the following section:

- *Directional stability* or *in-plane buckling*, which is the analysis of stability around the crosswise axis of the bridge. In addition, a *snap-through analysis* will also be performed;
- *Lateral stability* or *out-of-plane buckling*, which is the analysis of stability around the longitudinal axis of the bridge.

Both of them can be studied by a global analysis³. As written in EN 1993-1 (2005), Section 6.3: “Buckling resistance of Members” [33], a possible way to do that is to satisfy the following criterion:

$$\frac{N_{Ed} \cdot \gamma_M}{\chi \cdot f_{yk} \cdot A} + \frac{M_{x,Ed} \cdot \gamma_M}{\chi_{LT} \cdot f_{yk} \cdot W_x \cdot \left(1 - \frac{N_{Ed}}{N_{cr,x}}\right)} + \frac{M_{y,Ed} \cdot \gamma_M}{f_{yk} \cdot W_y \cdot \left(1 - \frac{N_{Ed}}{N_{cr,y}}\right)} \leq 1 \quad (2.15)$$

where χ is the reduction factor for the relevant buckling curve depending on the relevant cross-section and χ_{LT} is the reduction factor for lateral-torsional buckling. To satisfy the 2.15, χ must be defined. This factor depends on the type of section and the type of steel used and, as written in EN 1993-1, for axial compression in members, for the appropriate non-dimensional slenderness $\bar{\lambda}$ it can be determined from the relevant buckling curve shown in Figure 2.8 according to:

$$\chi = \frac{1}{\Phi + \sqrt{\Phi^2 + \bar{\lambda}^2}} \quad (2.16)$$

where Φ and $\bar{\lambda}$ can be calculated respectively as:

$$\Phi = 0.5[1 + \alpha(\bar{\lambda} - 0.2) + \bar{\lambda}^2] \quad (2.17)$$

$$\bar{\lambda} = \sqrt{\frac{A \cdot f_{yk}}{N_{cr}}} \quad (2.18)$$

Φ is a dimensionless value used to determine χ , and the imperfection factor α corresponding to the appropriate buckling curve can be obtained from the Eurocode, reported in Figure 2.9 and 2.10.

³A global analysis is a comprehensive assessment of an entire structure.

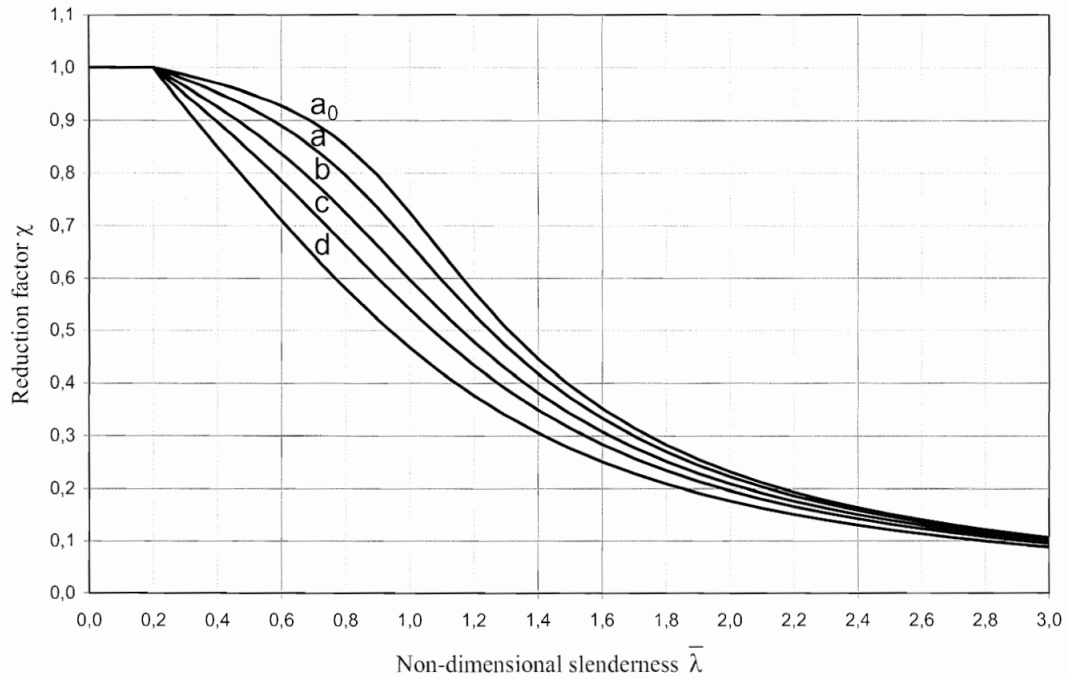


Figure 2.8: *Buckling curves, as reported in EN 1993-1 (2005) - “Buckling resistance of Members” [33].*

Buckling curve	a_0	a	b	c	d
Imperfection factor α	0,13	0,21	0,34	0,49	0,76

Figure 2.9: *Imperfection factor α for buckling curves, as reported in Table 6.1 of EN 1993-1 (2005) - “Buckling resistance of Members” [33].*

The value of N_{cr} depends on the type of buckling analysis conducted, as mentioned earlier, whether it is directional stability or lateral stability. The method for determining its value is explained in the following sections.

2.6.1 Directional Stability and Snap-Through Analysis

As mentioned before, directional stability concerns the stability around the crosswise axis of the bridge [21]. Therefore, a steady and stable position and alignment along its length must be ensured.

As reported in EN 1993-2 (2006), Annex D.3: “Arches Bridges” [35], the critical buckling load in the arch for in-plane buckling used to satisfy the Equation 2.15 is expressed by:

$$N_{cr} = \left(\frac{\pi}{\beta \cdot s} \right)^2 \cdot EI_x \quad (2.19)$$

where s is the half length of the arch, EI_x is the in-plane flexural stiffness of the arch

2. Background

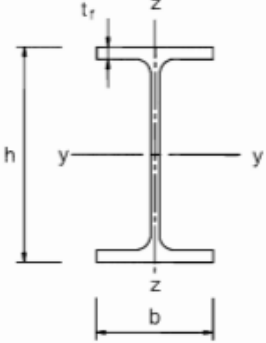
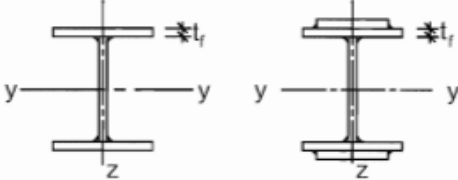

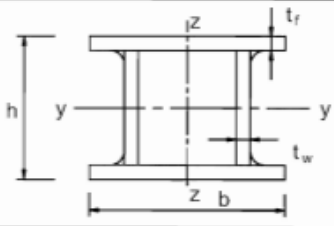
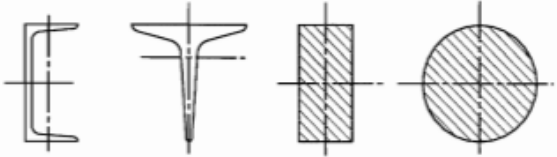

Cross section		Limits	Buckling about axis	Buckling curve	
				S 235 S 275 S 355 S 420	S 460
Rolled sections		$h/b > 1,2$	$t_f \leq 40 \text{ mm}$	y - y z - z	a a ₀
			$40 \text{ mm} < t_f \leq 100$	y - y z - z	b a
		$h/b \leq 1,2$	$t_f \leq 100 \text{ mm}$	y - y z - z	b a
			$t_f > 100 \text{ mm}$	y - y z - z	d c
Welded I-sections		$t_f \leq 40 \text{ mm}$		y - y z - z	b c
		$t_f > 40 \text{ mm}$		y - y z - z	c d
Hollow sections		hot finished		any	a a ₀
		cold formed		any	c c
Welded box sections		generally (except as below)		any	b b
		thick welds: $a > 0,5t_f$ $b/t_f < 30$ $h/t_w < 30$		any	c c
U-, T- and solid sections				any	c c
L-sections				any	b b

Figure 2.10: Selection of buckling curve for a cross-section, as reported in Table 6.2 of EN 1993-1 (2005) - “Buckling resistance of Members” [33].

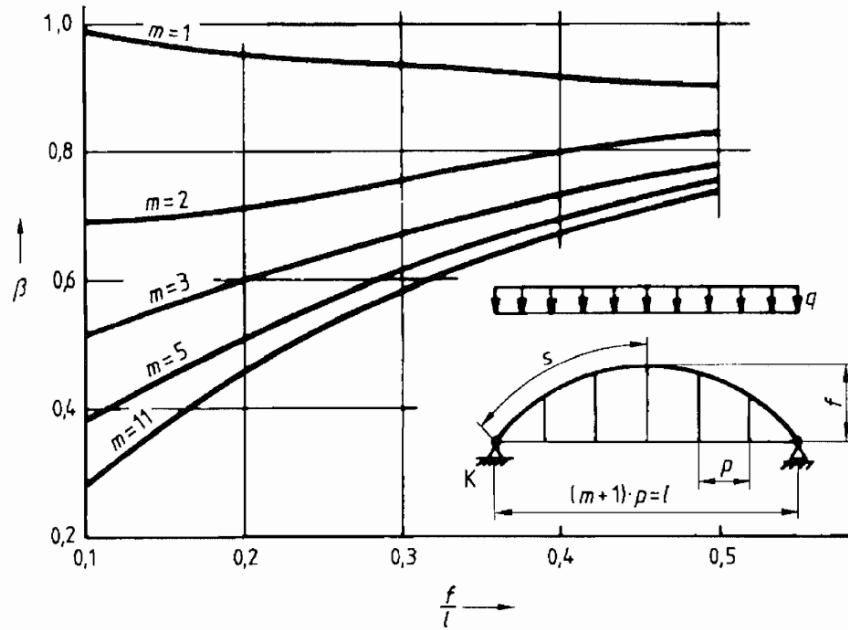


Figure 2.11: In-plane buckling factor β , as shown in EN 1993-2 (2006), Annex D.3 - “Arches Bridges” [35].

and β is the buckling length factor. For arches with a tension tie and hangers, the buckling factor β can be found in Figure 2.11.

Furthermore, a snap-through analysis must be conducted too. In the field of civil engineering, snap-through typically refers to a structural instability phenomenon that can occur in certain types of structures, most notably in arches, cables, and other flexible systems [36]. It is a sudden and often unexpected change in the shape or behavior of a structure due to changes in loading, deformation, or other external factors and is characterized by the sudden transition of a structure from one stable equilibrium position to another one through an unstable region in its load-deformation curve. This transition is often accompanied by a rapid and non-linear change in the structure’s shape or configuration. Because of this, verify its accuracy is crucial when designing tied-arch bridges.

As an example, let’s consider a generic elastic arch of a steel bridge. When a downward force F is gradually applied to the apex of the arch, it initially deforms in a stable manner. However, at a certain critical load, the arch suddenly flips to a new configuration, known as the *snap-through position*. This new position is also stable, but it is drastically different from the original shape of the arch. As an example, these two stable states are represented in Figure 2.12. In practice, the arch would not be able to reach the new configuration, resulting in the collapse of the structure instead. This phenomenon is due to the interaction of geometric non-linearity and the structural stiffness of the system [36], [37]. According to the EN 1993-2 (2006), Annex D.3: “Arches Bridges” [35], snap-through of arches may be prevented if the following criterion is satisfied:

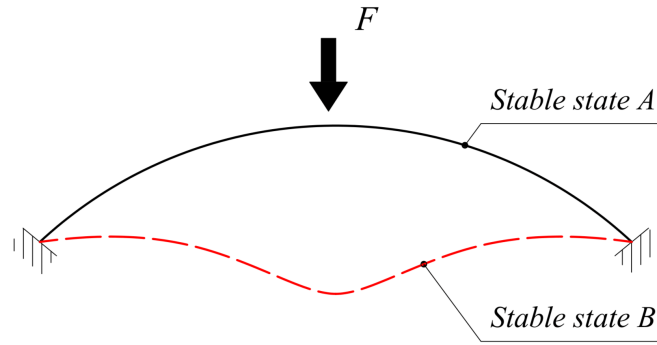


Figure 2.12: Snap-through stable states of a generic elastic arch under a downward force F gradually applied to its apex [36].

	f/l	0,05	0,075	0,10	0,15	0,20
	K	35	23	17	10	8
		319	97	42	13	6

Figure 2.13: The snap-through dimensionless K factor, as shown in Table D.5 of EN 1993-2 (2006), Annex D.3 - “Arches Bridges” [35].

$$tmp = l \cdot \sqrt{\frac{EA_a}{12EI_x}} > K \quad (2.20)$$

where A_a is the cross-sectional area of the arch, K is the snap-through dimensionless factor, f is the height of the arch and l is the projection length of the arch, generally equal to the deck length.

The value of the factor K can be found from Table D.5 in EN 1993-2 (2006), Annex D.3: “Arches Bridges” shown in Figure 2.13 and it depends on f/l and on the boundary conditions at the arch ends, which can be *double-articulated arch* or *non-articulated arch*.

2.6.2 Lateral Stability

An out-of-plane analysis must be performed to avoid the collapse of the structure given by horizontal actions like wind loads, seismic loads and, of course, live loads like moving vehicles. Specifically, tied-arch bridges are particularly susceptible to this phenomenon due to their distinctive shape. Therefore, the critical buckling load must be defined to satisfy the Equation 2.15. As written in EN 1993-2 (2006), Annex D.3: “Arches Bridges” [35], the critical buckling load in free standing arches for out-of-plane buckling is expressed by:

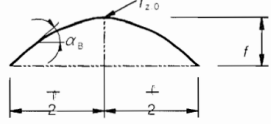
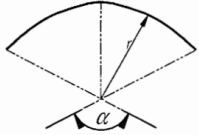
f/l	0,05	0,10	0,20	0,30	0,40	
I_z constant	0,50	0,54	0,65	0,82	1,07	
I_z varies $I_z(\alpha_B) = \frac{I_{z,0}}{\cos \alpha_B}$	0,50	0,52	0,59	0,71	0,86	

Figure 2.14: Out-of-plane buckling factor β_1 , as shown in Table D.6 of EN 1993-2 (2006), Annex D.3 - “Arches Bridges” [35].

Loading	β_2	Comments
conservative (The deck is fixed to the top of the arch)	1	
by hangers	$1 - 0,35 \frac{q_H}{q}$	
by posts	$\left[\overline{AC_1} \right] 1 + 0,45 \frac{q_{St}}{q} \left[\overline{AC_1} \right]$	

q total load
 q_H load part transmitted by hangers
 q_{St} load part transmitted by posts

Figure 2.15: Out-of-plane buckling factor β_2 , as shown in Table D.7 of EN 1993-2 (2006), Annex D.3 - “Arches Bridges” [35].

$$N_{cr} = \left(\frac{\pi}{\beta \cdot l} \right)^2 EI_y \quad (2.21)$$

where EI_y is the out-of-plane flexural stiffness of the arch and β is the buckling length factor. The factor β can be calculated as:

$$\beta = \beta_1 \cdot \beta_2 \quad (2.22)$$

where β_1 and β_2 can be found from the Eurocode in Table D.6 and D.7, also depicted in Figures 2.14 and 2.15 respectively.

2.6.3 First-Order and Second-Order Analysis

After defining N_{cr} for both in-plane and out-of-plane buckling, a global analysis is needed to verify their values [23]. Thanks to the EN 1993-1-1 (2005), Section 5.2: “Global Analysis” [33], it can be performed by following two different types of analyses:

- the *first-order analysis*, imposing equilibrium on the initial configuration of the structure;
- the *second-order analysis*, imposing equilibrium on the deformed configuration of the structure.

2. Background

	1	2	3			
			e_0 according to classification of cross section to buckling curve			
		shape of imperfection (sinus or parabola)	a	b	c	d
1			$\frac{s}{300}$	$\frac{s}{250}$	$\frac{s}{200}$	$\frac{s}{150}$
2			$\frac{\ell}{600}$	$\frac{\ell}{500}$	$\frac{\ell}{400}$	$\frac{\ell}{300}$

Figure 2.16: Imperfections for in-plane buckling of arches, as shown in Table D.8 of EN 1993-2 (2006), Annex D.3 - “Arches Bridges” [35].

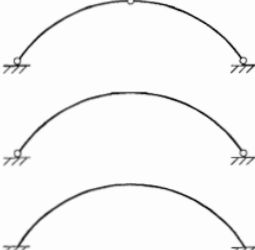

	shape of imperfection (sinus or parabola)	e_0 according to classification of cross section to buckling curve				
			a	b	c	d
		$\ell \leq 20 \text{ m}$	$\frac{\ell}{300}$	$\frac{\ell}{250}$	$\frac{\ell}{200}$	$\frac{\ell}{150}$
		$\ell > 20 \text{ m}$ $\ell_1 = \sqrt{20 \ell} [\text{m}]$	$\frac{\ell_1}{300}$	$\frac{\ell_1}{250}$	$\frac{\ell_1}{200}$	$\frac{\ell_1}{150}$

Figure 2.17: Imperfections for out-of-plane buckling of arches, as shown in Table D.9 of EN 1993-2 (2006), Annex D.3 - “Arches Bridges” [35].

The global analysis can be carried out with the first-order theory in cases where the effects of the deformations, on the instability phenomena and on any other relevant response parameters of the structure, can be considered negligible. For elastic analysis, this condition can be reached if the following relationship is satisfied:

$$\alpha_{cr} = \frac{F_{cr}}{F_{Ed}} \geq 10 \quad (2.23)$$

where α_{cr} is the critical buckling load multiplier that triggers the initial form of global instability, F_{cr} is the critical buckling load given by considering the initial elastic stiffness of the structure and F_{Ed} is the design load. By assuming this relationship, the buckling analysis can be satisfied when:

$$F_{Ed} \cdot \alpha_{cr} = F_{cr} \geq 10 \quad (2.24)$$

In case a second-order analysis is needed instead, we can take into account the bow imperfections⁴ in Figure 2.16 and 2.17 for in-plane and out-of-plane buckling respectively as explained in EN 1993-2 (2006), Annex D.3: “Arches Bridges” [35].

2.7 Carbon Dioxide Emissions in Steel Production

The problem of high carbon dioxide (CO₂) emissions is a critical issue stemming from human activities, primarily the burning of fossil fuels, deforestation, and industrial processes [3]. As CO₂ is a major greenhouse gas, its excessive release into the atmosphere contributes to the greenhouse effect, trapping heat and leading to global warming and climate change.

The environmental impact of various steel grades are assessed in terms of their CO₂ equivalent emissions. Hence, for each of them, the *Global Warming Potential* (GWP) must be defined [3], [4]. The GWP is a measure used to compare the potency of different greenhouse gases in terms of their ability to trap heat in the Earth’s atmosphere over a specific time period (20, 100 or 500 years). It is expressed as a factor relative to the warming potential of carbon dioxide, which is assigned a GWP of 1. Hence, the GWP serves as a tool to estimate the actual environmental impact characteristics of a structure.

Having established an exhaustive background, in the following chapter we are detailing our methodology, which includes a description of the case studied and the development of the optimization process.

⁴Bow imperfections are deviations or irregularities in a structural system to account for uncertainties.

3

Methods

The primary focus of this thesis is the development an algorithm used to assess the environmental impact of tied-arch bridges. After that, the algorithm is employed to optimize the bridge structure through the examination of various alternative designs proposed by minimizing the steel usage, resulting in costs and CO₂ emissions reduction. The purpose of our algorithm is not to produce complete designs or accurate estimates of the results; rather, it should point in the right direction and help the designer to quickly find a good solution. To reach this goal, an existing tied-arch bridge was taken as the focus of this study.

In this chapter, we introduced the tied-arch bridge studied. After that, we explained the optimization process adopted, focusing the attention on its key steps.

3.1 Case Study of an Existing Tied-Arch Bridge: Bridge over the Carpi's Highway Station

The bridge studied in this thesis is the bridge over the Carpi's highway station. It is an existing tied-arch bridge that has been designed conventionally, located in the city of Carpi (MO), in Italy. The design was carried out according to the Eurocodes by the company Autostrada del Brennero S.p.A. in 2007. Its main geometrical aspects are listed in this section. In Figure 3.1, 3.2 and 3.3 more detailed measurements of deck's and arch's cross-sections are listed.

The bridge features a single-span structure with a calculated span of 65 meters. The steel orthotropic deck is 16.20 meters wide and is suspended by 14 hangers from a central steel arch that is 6.55 meters in height, effectively eliminating thrust, with an approximate rise-to-span ratio of 1/10. The deck is torsionally rigid, consisting of two diaphragm boxes connected to cantilever arms. The structural height of the deck varies with a 2.5 % transverse gradient, reaching a maximum of 1.635 meters in the central area where the hangers are anchored. The cross-section includes two 0.75-meter-wide reinforced concrete side girders with safety rails and plexiglass protections. There is also a central 1.60-meter-wide reinforced concrete girder from which the arch extends, and two carriageways with a usable width of 6.55 meters.

In the following sections, we outline the steps of our algorithm used to develop alternative designs from the initial one, summarized in the flowchart diagram depicted in Figure 3.4.

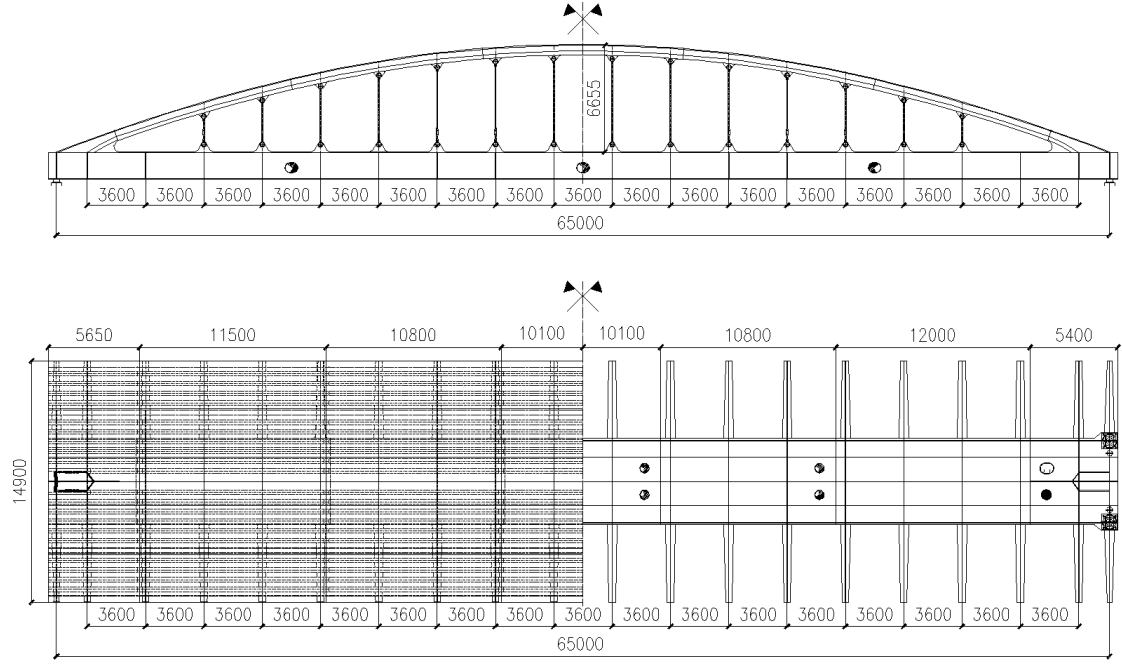


Figure 3.1: *Elevation showing the original design of the bridge over the Carpi's highway station, longitudinal profile and deck plan respectively.*

3.2 Modeling the Optimization Problem

Designing a tied-arch bridge is a multi-step iterative process where structural solutions and various parameters are carefully considered. Formulating optimization problems for such complex tasks can be challenging, often requiring extensive numerical modeling for each iteration.

The initial step in generating a new alternative design for the studied bridge involves defining whether a parameter is a constant or variable in our algorithm. After that, we proceed to assign the constraints and the objective function.

3.2.1 Design Variables

Minimizing the quantity of design variables significantly impacts the number of iterations required to attain an optimal solution. The following quantities of size and shape have been chosen as design variables, capable of influencing the amount of steel usage, as well as costs and CO₂ emissions of the arch:

- Cross-sectional area of the Arch (A_a);
- Height of the arch (f).

The height of the arch, influenced by the f/l ratio, fundamentally characterizes the structure of arch bridges. These quantities are the independent variables in our optimization problem since they are not dependent on any other variable. The user shall set the value of f as the first step of our algorithm. Hence, the height of the

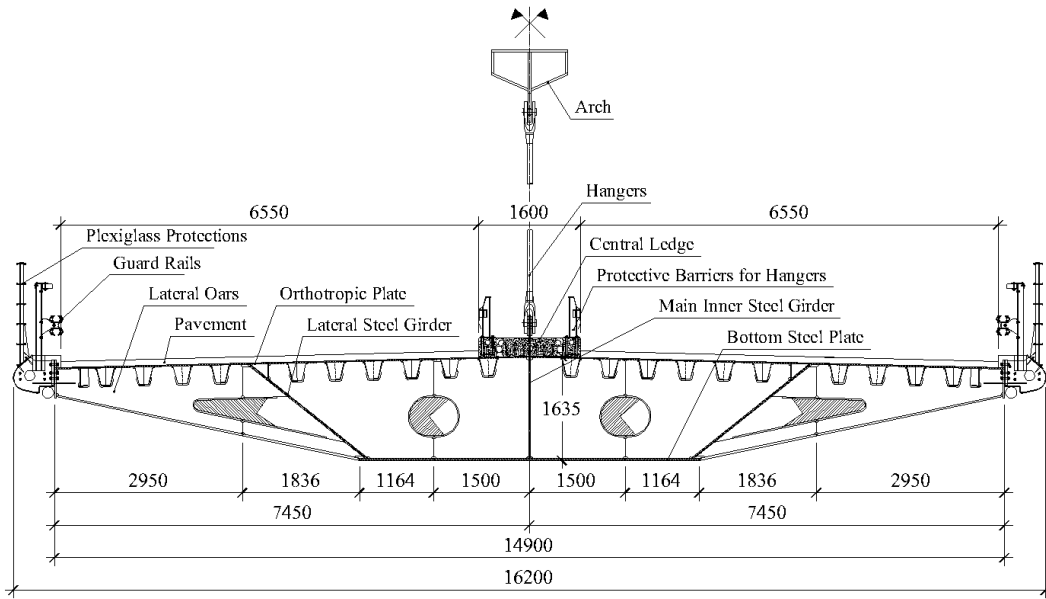


Figure 3.2: Elevation showing the original design of the bridge over the Carpi's highway station, transversal section.

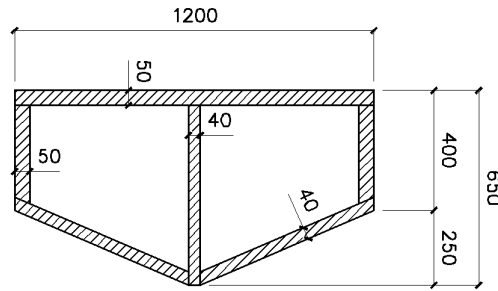


Figure 3.3: Elevation showing the original design of the arch's cross-section of the bridge over the Carpi's highway station. The section is constant along its entire development.

arch characterises each alternative design.

3.2.2 Dependent Variables

The moment of inertia about the x and y axes calibrates in-plane and out-of-plane buckling analyses, respectively, both of which depend on the arch's cross-sectional area. The stresses acting on the bridge are also dependent variables calculated using a finite element model, which will be explained in the next Section, considering the geometric and mechanical characteristics of the bridge structure. These characteristics encompass elements such as the cross-sectional area of the arch, a key design variable. The resistances, explained in Section 2.5, are variables that depend on both the arch and deck cross-sectional areas. Finally, to understand the geometry-dependent variables, let's consider the right triangle $\triangle AOB$ in Figure 3.5. The first parameter

Table 3.1: *Dependent variables with their reference units.*

Parameter	Unit
Moment of inertia about the x -axis	m ⁴
Moment of inertia about the y -axis	m ⁴
Arch compressive stress/resistance	kN
Deck tensile stress/resistance	kN
Deck stress/resistance shear force	kN
Deck stress/resistance bending moment	kNm
Angle from the center of the arch	°
Radius	m
Circumference	m
Arch length	m

$$6.89 : 48 = f : \theta \quad (3.1)$$

where f is the arch height assumed as a design variable. Hence, the angle θ can be calculated as:

$$\theta = \frac{f \cdot 48}{6.89} \quad (3.2)$$

Once we know θ , the radius r is trivial to calculate as well:

$$r = \frac{L}{2} \cdot \frac{1}{\sin(\theta/2)} \quad (3.3)$$

After that, the circumference C can be simply found via:

$$C = 2 \cdot \pi \cdot r \quad (3.4)$$

Finally, the arch length can be determined thanks to the following proportion:

$$S = \frac{C \cdot \theta}{360} \quad (3.5)$$

Therefore, all these geometry parameters depend on the problem geometry, and our algorithm automatically calculates them once the design variables and preassigned parameters are defined. The aforementioned chosen dependent variables are listed in Table 3.1.

Table 3.2: *Preassigned parameters which the user can override with their default values and units.*

Parameter	Default value	Unit
Steel density	7850	kg/m ²
Nominal characteristic yield strength	355000	kN/m ²
Young modulus	2.1×10^8	kN/m ²
Cost per kilogram for steel grade S355	0.72	€/kg
Global Warming Potential (GWP)	2.044	
Bridge length	65	m
Deck cross-sectional area	0.618	m ²
Deck modulus of resistance	7.80	m ³
Number of hangers	14	
Hanger nominal diameter	0.072	m

3.2.3 Preassigned Parameters

Our optimization problem primarily involves treating most of its quantities as preassigned parameters with fixed values. In this approach, we need to minimize the number of design variables to reduce the required number of iterations for finding an optimal solution within a practical timeframe. Each of these preassigned parameters is user-definable and they are listed in Table 3.2. We opted not to vary the type of material used but to intervene only on the geometries of the arch. Therefore, the steel considered is the steel grade S355. Skoglund *et al.* [4] report that the GWP of steel grade S355 is equal to 2.044, while its cost in euros per kilogram stands at 0.72. The GWP value does not consider any recycling of scrap metal.

3.2.4 Objective Function

Our objective function aims to provide the user with three values: the amount of steel (in kilograms) used in constructing the bridge arch, the associated cost (in euros), and the quantity of CO₂ emitted (in kilograms). Following Skoglund *et al.* [4], these values can be calculated as follows:

$$W_{tot,a} = \rho \cdot A_a \cdot S \quad (3.6)$$

$$C_{tot,a} = \rho \cdot A_a \cdot C_a \cdot S \quad (3.7)$$

$$CO_{2eqe,a} = \rho \cdot A_a \cdot GWP \cdot S \quad (3.8)$$

where ρ is the unit weight of the steel (or steel density), S is the length of the arch, C_a is the cost per meter of steel and GWP is the global warming potential related to that steel grade. While it might initially appear as a multi-objective optimization,

in reality, $W_{tot,a}$, $C_{tot,a}$ and $CO_{2eq,a}$ vary proportionally with the common factors A_a and S , where A_a is a design variable and S depends on f , which is also a design variable. Therefore, by diminishing or augmenting the arch cross-sectional area or the arch height, the Equations 3.6, 3.7 and 3.8 will diminish or augment as well, collapsing into a single objective optimization.

3.2.5 Constraints

To classify a constraint, we adopted the penalty method reported in Section 2.1.3. All selected constraints are based on the resistance and stability analyses discussed in Sections 2.5 and 2.6, respectively. Furthermore, the designer has the flexibility to choose the range values of the arch height and cross-sectional area.

3.3 Parametric Shape Modeling and Sizing Cross-Sections of the Arch

Since the optimization study conducted in this thesis primarily focuses on the bridge's arch, it is necessary to define an appropriate shape and cross-section of the arch at each iteration. To address this, we followed a parametric approach, summarized in the flowchart diagram shown in Figure 3.6 and discussed in the following subsections, where arch height, deck length and a discretization of both arch and deck are required as inputs, having the parametrization of the arch shape and cross-sections, as well as its cross-sectional area as outputs.

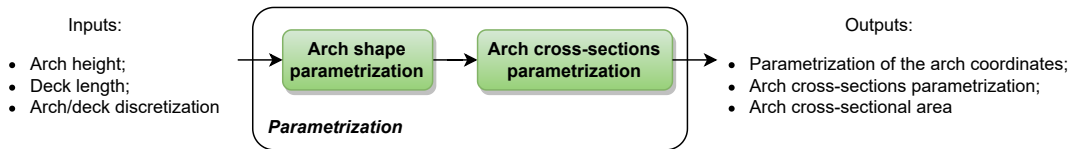


Figure 3.6: Flowchart diagram of the parametrization step.

3.3.1 Arch Shape Parametrization

The case study carried out in this thesis concerns the arch of the bridge, so its shape must be able to change at each iteration while the deck remains geometrically unchanged. To facilitate this, a parametric modeling approach for the arch is required. Therefore, our goal is to assign a function to each z -coordinate of the arch's points, describing the arch's shape instead of using fixed values, as illustrated in Figure 3.7.

By assuming to dispose a Cartesian system of axes with its origin in one of the two ends of the bridge and by assuming to dispose the bridge along the x -axis and its elevation along the z -axis, we can discretize the length L of the deck and the corresponding length S of the arch along x into l equal portions. In this way, we obtain $l + 1$ points x_0, x_1, \dots, x_l . Let's then assume that the value of each of these points corresponds to their subscript, *i.e.* $x_0 = 0, x_1 = 1, \dots, x_l = l$. Now, to obtain the optimum shape of the arch, we need a function that describes the pure bending

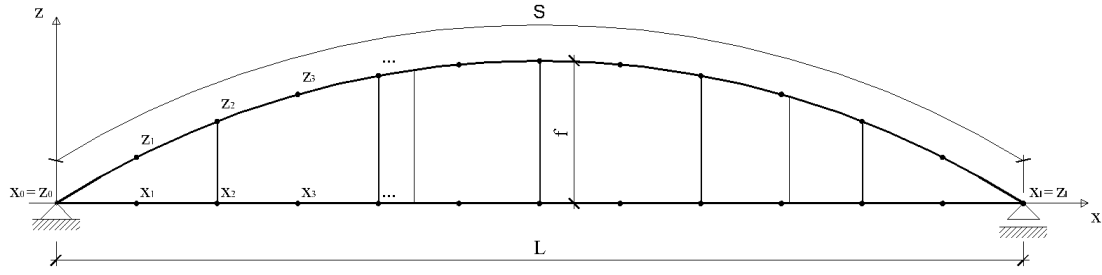


Figure 3.7: Arch shape parametrization. A function is assigned to each z -coordinate instead a fixed value.

of a generic simple supported beam subjected to a uniformly distributed load, $w(x/l)$ [38], which can be defined as follows:

$$w(x/l) = \frac{qL^4}{24EI} \cdot \left[\left(\frac{x}{l} \right)^4 - 2 \left(\frac{x}{l} \right)^3 + \frac{x}{l} \right], \quad x = 0, 1, 2, \dots, l \quad (3.9)$$

where x is the x -th point that describes the arch (or the deck), l is the total number of points describing the arch (or the deck) and q is the applied transverse load (in z direction);

If we want the rise value f of the arch in the middle of the deck, that is, its maximum height, we just have to replace x with $l/2$, so:

$$f = w(0.5) = \frac{5qL^4}{384EI} \quad (3.10)$$

At this point, to find the z -coordinate of each point of the arch, we introduce a scaling factor ϕ defined as follows:

$$\phi = \frac{16}{5}f \quad (3.11)$$

Finally, the function used to find each- z coordinate becomes:

$$z_x(x/l) = \phi \cdot \left[\left(\frac{x}{l} \right)^4 - 2 \left(\frac{x}{l} \right)^3 + \frac{x}{l} \right], \quad x = 0, 1, 2, \dots, l \quad (3.12)$$

In this way, we assigned a function to each z -coordinate of each point of the arch, instead of a fixed value.

To give an example, let us consider a discretization of a given tied-arch bridge obtained by setting $l = 36$, so that it is defined by $l + 1 = 37$ points. The two points that define the supports located at the ends of the bridge, *i.e.*, the points called *number 0*, in the origin of the axes, and *number 36*, are included in the count and their z -coordinates are obviously both equal to 0. The function that describes the z -coordinate of the second point of the arch can be now written as:

$$z_1(1/l) = \phi \cdot \left[\left(\frac{1}{36} \right)^4 - 2 \left(\frac{1}{36} \right)^3 + \frac{1}{36} \right]$$

and so on for the rest of the points.

3.3.2 Arch Shape for the Second-Order Analysis

As specified in Subsection 2.6.3, *First-Order and Second-Order Analysis*, when the buckling load multiplier exceeds the value of 10, a second-order analysis is required and a deformed shape must be modeled by calculating the eccentricity e_0 , as presented in Figure 2.17. This can be achieved in a manner similar to what was described in Subsection 3.3.1, *i.e.*, by parametrizing the arch based solely on the f variable. To simplify the analysis, we choose to replicate only one out-of-plane deformed configuration.

The eccentricity e_0 corresponds to the orthogonal translation of the apex of the arch. When viewing the structure from a transverse perspective, the projections of the arch in both deformed and undeformed configurations can be seen as straight lines that form a right triangle with the base equal to the eccentricity, as depicted in Figure 3.8. To parameterize the deformed configuration, it is necessary to define not only the x and z coordinates mentioned in Subsection 3.3.1, but also the y coordinate, which represents the transverse direction of the arch. The function describing the deformed configuration straight line is the equation of a straight line passing through the origin [39]:

$$z(y) = m \cdot y \tag{3.13}$$

where m is the gradient, given by:

$$m = \tan(\alpha) \tag{3.14}$$

The angle α is derived by trigonometry knowing that:

$$\frac{\pi}{2} - \alpha = \arcsin\left(\frac{e_0}{f}\right) \tag{3.15}$$

Hence, the function to assign to each y -coordinate is:

$$y(z) = \frac{z}{\tan(\alpha)} \tag{3.16}$$

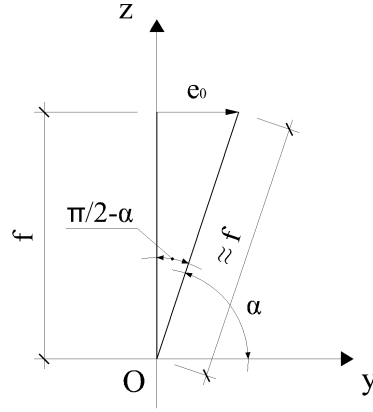


Figure 3.8: *Second-order arch shape parametrization, transversal view.*

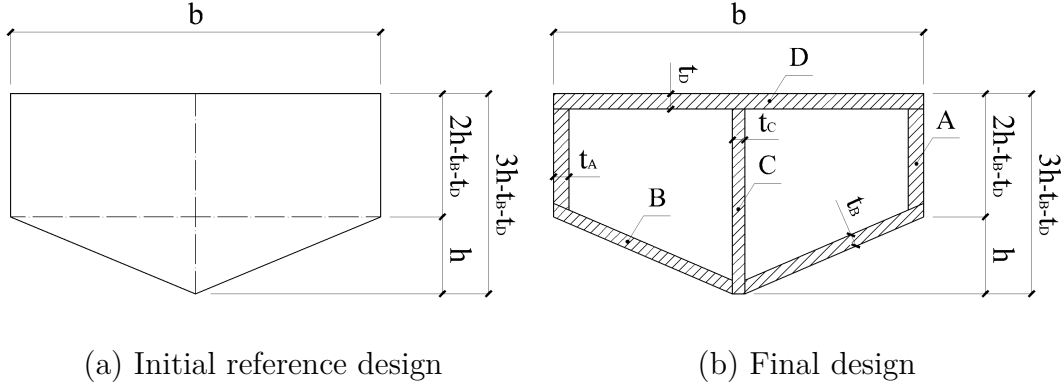


Figure 3.11: *Reference and final design of arch's cross-section.*

3.3.3 Arch Cross-Sections Parametrization

After defining the arch's shape, the next step is determining the appropriate cross-section. The value of the cross-sectional area, along with the arch length, significantly influences the final outcome of our objective function, as we discussed in Subsection 3.2.4, *Objective Function*.

Before determining the suitable cross-sectional area for the arch, several preparatory steps are required. Initially, we must establish the shape of the cross-section. To replicate a shape similar to the original design, reported in Figure 3.3, it is necessary to discretize it into simpler geometric forms. Hence, we opted for two simple geometries: a rectangle and a triangle, with shared characteristics. Specifically, the long side of the rectangle corresponds to the base b of the triangle, and the short side of the rectangle is set equal to twice the height h of the triangle, as shown in Figure 3.11 (a). It is important to note that the actual section is not solid but rather hollow, composed of multiple steel plates with varying thicknesses welded together. Its final design is shown in Figure 3.11 (b).

To proceed, we now need to define the types of plates used and, for each type, determine their thickness. These thicknesses, in conjunction with the parameters b and h introduced earlier, collectively form the set of parameters that the designer can

Table 3.3: *Parameters used for the parametrization of the arch cross-section, including their acronyms and units.*

Parameter	Acronyms	Unit
Base of the triangle	b	m
Height of the triangle	h	m
Plate thickness A	t_A	m
Plate thickness B	t_B	m
Plate thickness C	t_C	m
Plate thickness D	t_D	m

adjust during each iteration in order to automatically calculate the cross-sectional area of the arch. The lengths of each plate is naturally constrained by the parameters b and h . Four types of plates A, B, C, and D were categorized as shown in Figure 3.11. As a result, the parametrization of the arch cross-section comprises six parameters, as listed in Table 3.3. Each plates have a rectangular section, except the two Plate B in Figure 3.11, which are trapezoidal. Despite that, we approximate them as rectangular when we calculate their areas for simplicity, resulting in a negligible error.

3.4 Finite Element Model (FEM)

After defining the shape and cross-section of the arch, the next step is to model the structure using an external finite element model that allows us to recreate a three-dimensional model of a given bridge in which the moments of inertia I_x , I_y and the stresses acting on it can be found. Hence, we opted to exploit Strand7[®], version R.2.4.6, to accomplish this task, modeling the deck, arch and hangers. For each of them, sections, material and mechanical properties were chosen and the arch was parameterized as reported in Section 3.3, *Parametric Shape Modeling and Sizing Cross- Sections of the Arch*. However, the structural analyses focused solely on the arch and deck, neglecting the hangers, which are particularly susceptible to fatigue¹. For a more in-depth analysis, please refer to [40].

Figure 3.12 summarizes the if-else, which describes how the main components of a given bridge were designed for the finite element model and the loads that were applied in order to directly obtain the moments of inertia and the stresses. If a second-order analysis is required instead, a parametrization of the arch shape is conducted as explained in Subsection 3.3.2, *Arch Cross-Sections Parametrization*.

¹Fatigue is a material degradation process which can be studied by a specific structural analysis used to determine whether a structure will fail after a certain number of repeated loadings.

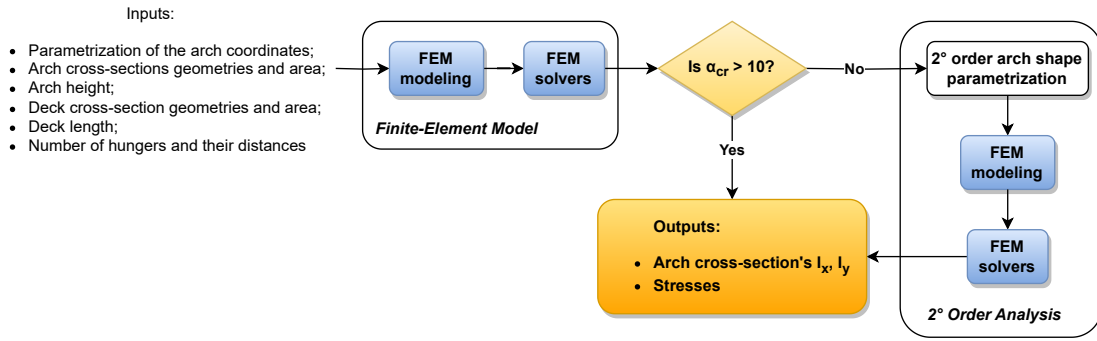


Figure 3.12: *If-else statement of the FEM step.*

3.4.1 FEM Modeling

The hangers, the deck and the arch of the bridge must be modeled within the finite element model by assigning them well-defined characteristics and properties. The suspension hangers of the bridge are bars Macalloy M76 [41] with a nominal diameter of 72 millimeters, so they were modeled as truss elements having that diameter. The truss elements were used as tension or compression members. A truss element is one dimensional, typically long and slender with axial forces and it is used for simulating axial deformation. The deck instead was modeled as a beam element. In particular, it is modeled as a box girder made of various steel components welded together, such as [42]:

- two main lateral steel girders;
- one main inner steel girder;
- one orthotropic superior plate²;
- one bottom steel plate.

Furthermore, lateral oars are typically used as crossbeams to support the extension of the road surface above the orthotropic plate. In order to reduce the number of elements and simplify the problem, we decided to omit the lateral oars. Instead, the box girder was modeled as a standard beam made of a series of beam elements having a pre-assigned cross-section, with the finite element model automatically calculating the cross-sectional area, moments of inertia about the x and y axes, and torsion constants. Each arch beam consists, instead, of multiple welded metal plates as early said, and the section is pre-assigned but subject to variation in each iteration to find the optimal area value, as illustrated in Subsection 3.3.3, *Arch Cross-Sections Parametrization*. Finally, the abutments were modeled with both fixed and sliding bearing restraints.

²An orthotropic plate is a structural element with varying material properties in different directions, providing unique mechanical characteristics.

3.4.2 Acting Loads

While structural dead loads are automatically calculated in Strand7[®], non-structural dead load must be assigned considering all bridge's non-structural elements. Furthermore, a transient load moving along the deck was modeled using the Strand7[®] Moving Load module, considering an oversize load³ [43]. This load was distributed in nine-axle load groups in which each group was treated as a single point force of various intensities. Thanks to this moving load, four beam response variables⁴ were defined, and an influence line study was conducted, according to Section 2.4, *Influence Lines*, to determine the bending moment, shear force, and tension and compression loads acting on the bridge. We employed beam response to assess the influence that a point force or moment applied anywhere in the structure has on the selected quantity along the beam. Thus, they provide answers to the following question: what is the load position that maximizes a specific stress acting on the bridge?

3.4.3 FEM Solvers

Once the structure has been modeled and the acting loads have been defined, it is possible to start the FEM solvers in Strand7[®], that are the load influence, the linear static solver and the linear buckling solver. The first solver is the load influence [44], used to determine the influence lines or, as mentioned in the previous subsection, the effects that a unit load has on a specific response variable. From this analysis, new load configurations are identified, which are implemented in the subsequent solver, that is the linear static solver [45], in which it is assumed that the behavior of the structure is linear and the load is static. The linear static solver computes and assembles the element stiffness matrices, along with equivalent element force vectors and external nodal force vectors. In the final step of this assembly procedure, the following linear system of equilibrium equations is formed:

$$[K]\vec{d} = \vec{P} \quad (3.17)$$

where $[K]$ is the global stiffness matrix, \vec{d} is the unknown nodal displacement vector and \vec{P} is the global nodal load vector.

Finally, a linear buckling analysis is carried out to determine the critical buckling load multiplier by solving the following eigenvalue problem [46]:

$$[K]\vec{x} = \alpha_{cr}[K_g] \quad (3.18)$$

where \vec{x} is the buckling mode vector, α_{cr} is the buckling load factor and $[K_g]$ is the global geometric stiffness matrix.

³An oversize load can be, for example, a truck that exceeds the standard legal size limits for transportation on roads.

⁴A response variable is a quantity or parameter calculated as a result of structural analysis.

The linear static results are used for resistance analysis, while the critical buckling load multiplier is used for buckling analyses as part of the iteration problem of arch cross-sectional sizing parametrization outlined in Subsection 3.3.3.

3.5 Stability Analyses

We performed the snap-through analysis, in-plane buckling analysis and out-of-plane buckling analysis in our algorithm as indicated in Section 2.6 in order to satisfy the Criteria 2.15 and 2.20. If each check is satisfied, the algorithm ensures the stability safety. Otherwise, we must resize the arch cross-sections by entering an iterative process as illustrated in the for-loop in Figure 3.13.

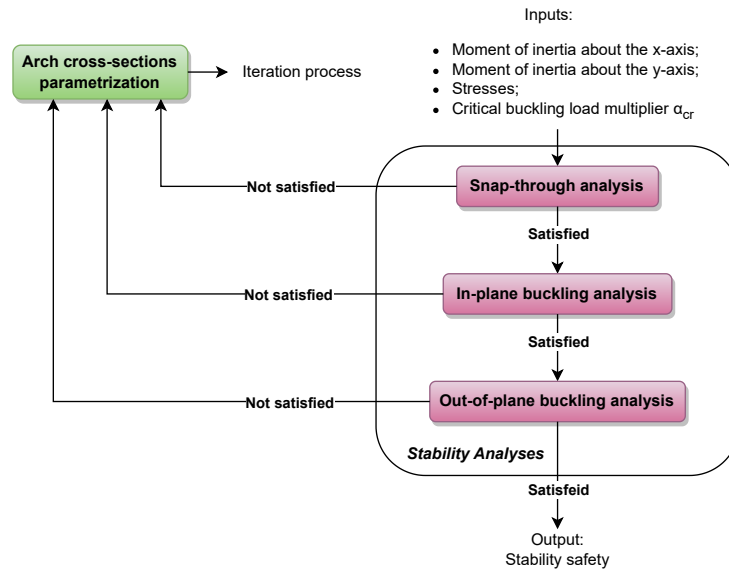


Figure 3.13: *For-loop of the stability analyses step.*

3.6 Python Development

The final step of our algorithm employs Python, version 3.10.12. After the variables and constants have been defined, we implement the snap-through function and the objective function. The snap-through function is used to add a constraint to the optimization problem, while the objective function serves us to finally assess the environmental impact of a given tied-arch bridge and then define whether the alternative proposed arch configurations results in steel and cost savings, as well as CO₂ emissions reduction. The algorithm calculates the objective function as shown in Subsection 3.2.4, *Objective Function*, resulting in calculating the Equations 3.6, 3.7 and 3.8, as well as the snap-through K value, in line with the Criterion 2.20 described in Subsection 2.6.1. Finally, we apply the constraints, resulting in resistance and snap-through analysis: if the constraints are satisfied, the algorithm calculates the results of the objective functions; conversely, the penalty is triggered, as indicated in Subsection 2.1.3, entering in the iterative for-loop as depicted in Figure 3.14.

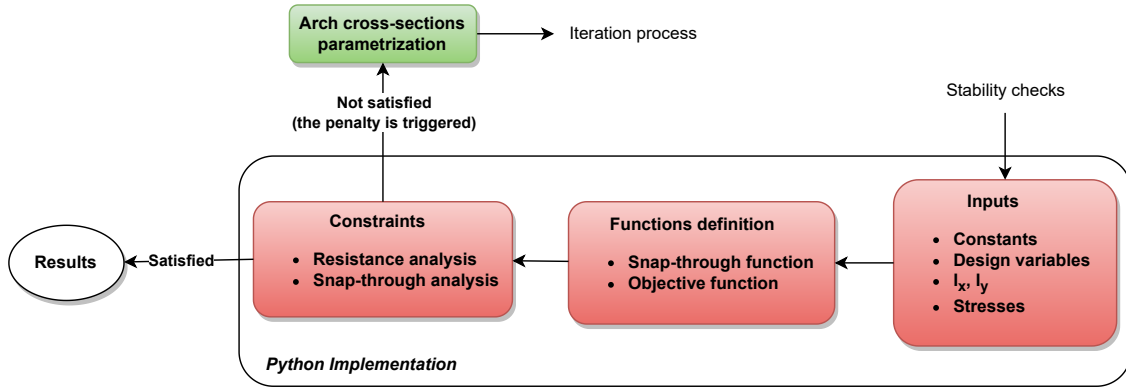


Figure 3.14: For-loop of the Python implementation step.

3.6.1 Constants, Dependent Variables and Design Variables

The initial step in the execution involves inputting the constants listed in Table 3.2, along with their respective values, into the algorithm. Subsequently, the user shall incorporate the most suitable values for the design variables identified in iterative processes, as well as the parameters that were generated as output at each iteration, as presented in Table 3.1. These parameters, together with the design variables, constitute the values that the designer needs to manipulate within the algorithm at each iteration. Additionally, the preassigned parameters must be defined.

3.6.2 Functions Definition

After defining the constants and manual variables, we need to specify how the parameter K varies for snap-through verification. As described in Subsection 2.6.1, this is determined based on a table, depending on the f/l ratio's value. In Python, this operation can be executed using two functions that determine the value K based on the input parameter f . The first of them takes three arguments, x , low , and $high$, and essentially finds which of the two extremes (low or $high$) is closer to the input value x and returns that extreme. This function calculates the middle point between low and $high$ by taking the absolute difference between them and dividing it by 2 and then adding low . This middle point is stored in a variable called p_{middle} :

$$p_{middle} = \left| \frac{low - high}{2} \right| + low \quad (3.19)$$

The function then compares the value of x with p_{middle} . If x is greater than or equal to p_{middle} , it returns $high$, otherwise, it returns low .

The second function takes the input parameter f and calculates the f/l ratio (remembering that l is a constant). Then, a dictionary⁵ that maps specific values of the ratio to corresponding values of K , which are reported in Figure 2.13. Finally, the function checks the value of the ratio f/l against the predefined ranges and

⁵A dictionary is an unordered collection of key-value pairs where each key is unique and used to access its associated value.

returns the corresponding value of K based on the range in which that ratio falls in, determining whether it is an articulated or a non-articulated arch. Following are the conditions for the non-articulated arch configuration:

- if $f/l \leq 0.05$, it returns the value of K associated with 0.05 in the dictionary, so the lowest value;
- if $f/l \geq 0.2$, it returns the value of K associated with 0.2 in the dictionary, so the highest value;
- if $0.05 \leq f/l \leq 0.075$, it returns the value of K associated with the closer end point (either 0.05 or 0.075) using the first function;
- similarly, it checks for other ranges (0.075 to 0.1, 0.1 to 0.15, and 0.15 to 0.2) and returns the value of K associated with the closer end point for each range.

After the snap-through functions, the objective function can be evaluated with the design variables as arguments. Inside the objective function we must define the constraints as explained in 2.1.3, specifically, the resistance and snap-through analysis as well defined in Section 2.5 and Subsection 2.6.1. In particular, for the snap-through analysis, the program calculates the value K by calling the second function explained above. It then calculates the temporary value tmp used to satisfy the Criterion 2.20.

3.6.3 Python Constraints

The algorithm applies a series of constraint checks to verify whether the snap-through and resistance analyses have been satisfied. If any of the constraints are violated, a very high penalty is assigned. The algorithm then identifies the specific check that was unsuccessful, enabling the user to quickly find the issue and intervene in a more targeted manner during the resulting iteration process where, in such cases, the user will need to resize the cross-sections of the arch. The constraints include comparisons between the calculated parameters, specifically, resistance and the K value, and stresses acting on the bridge. Otherwise, if none of the constraints are violated, the script proceeds to calculate and return the values of the total weight, cost, and CO₂ equivalent emissions for the arch as strings.

3.6.4 Reporting of the Results

The final step of the algorithm involves reporting results. In this step, the script reports comparisons between resistance values and stresses acting on the bridge, as well as the snap-through K factor values. After that, the algorithm indicates whether verification occurred or not. Additionally, it reports the values of the objective function. Furthermore, our algorithm performs a conditional check: if the emitted CO₂ value is less than the CO₂ emitted for the initial arch configuration, it informs the user that savings were achieved. Then, it calculates and reports the following information:

- the amount saved steel in kilograms compared to the initial arch configuration;

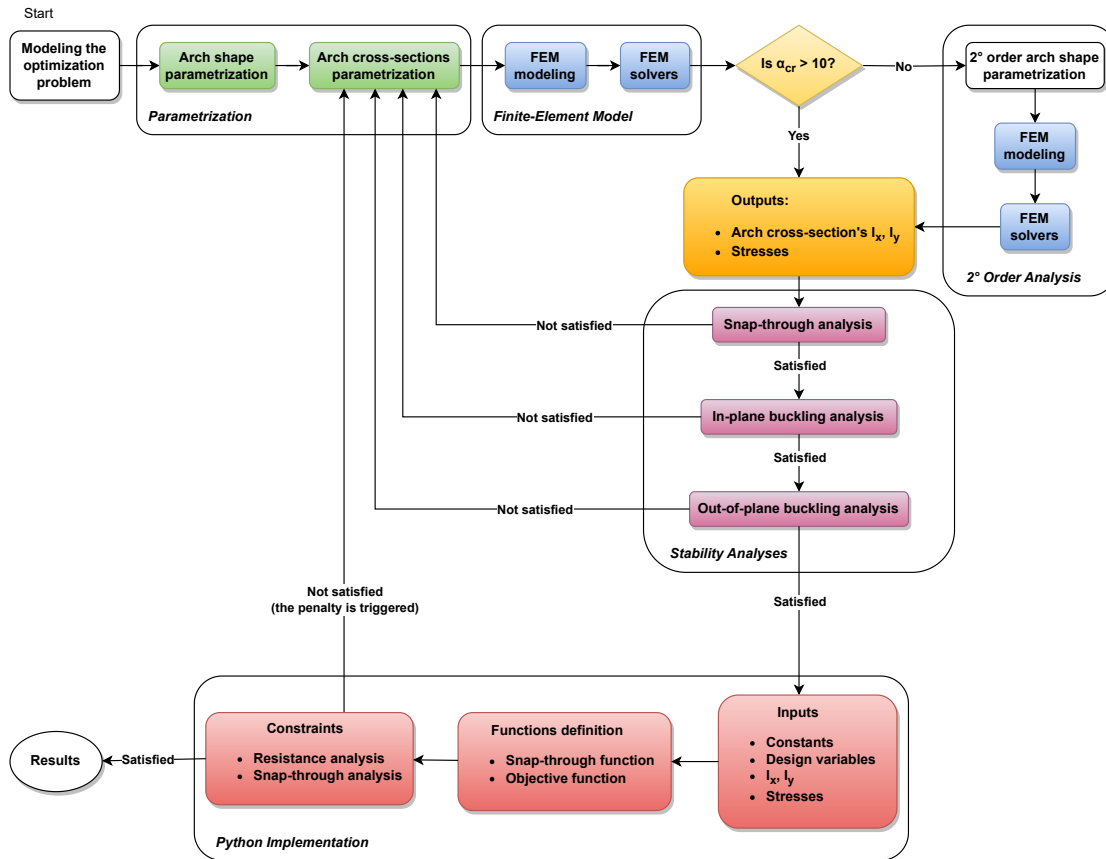


Figure 3.15: Flowchart diagram of the optimization problem.

- the saved cost in euros compared to the initial arch configuration;
- the saved CO₂ emitted in kilograms compared to the initial arch configuration;
- the percentage of the objective function score, that is, the saving percentage.

Since the objective function is composed of three functions that vary proportionally with the common factor A_a and S , as explained in Subsection 3.2.4, the amount of steel usage, cost, and CO₂ emitted exhibit proportional variations. Therefore, a single percentage of the objective function score is required. However, if the emitted CO₂ value is greater than the CO₂ emitted for the initial arch configuration, it warns the user that no savings were achieved, and the following information is reported:

- the amount of excessive steel in kilograms compared to the initial arch configuration;
- the excessive cost in euros compared to the initial arch configuration;
- the excessive CO₂ emitted in kilograms compared to the initial arch configuration;
- the percentage of the objective function score, that is, the spending percentage.

The entire proposed algorithm is explained in the flowchart diagram shown in Figure 3.15.

4

Results and Discussion

In the previous chapter, we developed an algorithm to assess and optimize the environmental impact of tied-arch bridges. The optimized designs shall be not only cost-effective and environmentally friendly, but also feasible and realistic. This chapter is structured into three sections: first, we report the objective function results of the bridge studied in Section 3.1, then we present five distinct conceptual designs that deviate from the original design. Finally, we report the objective functions results of these conceptual designs, and a final discussion concludes the chapter.

4.1 Objective Function Results for the Reference Design

For the original studied bridge, each parameter of Equations 3.6, 3.7 and 3.8 listed in Subsection 3.2.4, *Objective Function*, is already known from the reference documentation, thus we can quickly determine its objective function scores, listed in Table 4.1.

Table 4.1: Arch cross-sectional area (A_a) and objective function results (steel weight $W_{tot,a}$, cost $C_{tot,a}$ and carbon dioxide emitted $CO_{2eqe,a}$) for the reference design (R.D).

Design	f/l	A_a (m ²)	$W_{tot,a}$ (kg)	$C_{tot,a}$ (€)	$CO_{2eqe,a}$ (kg)
R.D.	0.10	0.163	85 654	61 671	175 076

4.2 Proposed Conceptual Designs

After analyzing the original case study, the next step involves optimizing it by evaluating various configurations with different arch shapes and cross-sections, referred to as *Conceptual Designs*. Before delving into the detailed exploration of conceptual designs, we explain some common design choices adopted for each case study. Afterwards, five illustrative scenarios are discussed.

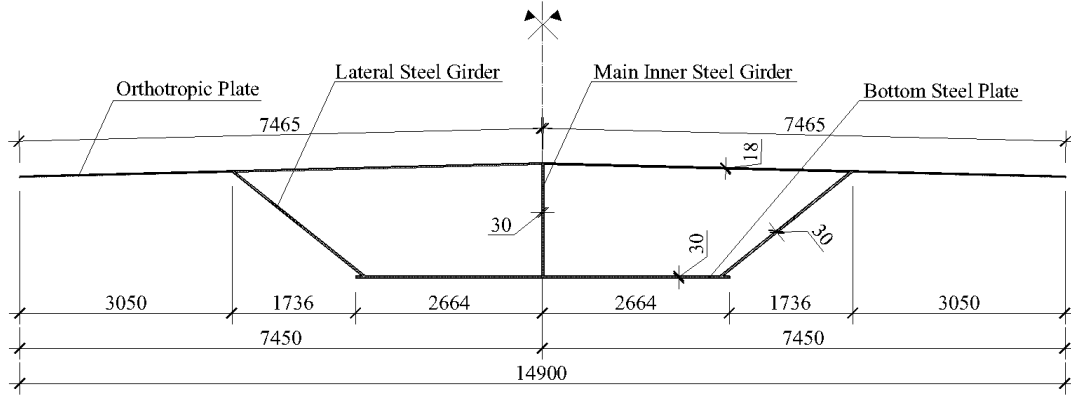


Figure 4.1: Elevation showing the box girder section of the reference bridge over the Carpi's Highway Station, including their geometries expressed in millimeters. We decided to leave the deck shape unchanged.

4.2.1 Common Structural Aspects

Several common design choices were incorporated in the development of the conceptual designs. Since we focus on the arch of the bridge, we decided to leave the shape of the deck unchanged throughout the entire optimization process, as suggested in Section 3.4, *Finite Element Model (FEM)*. The deck's adopted geometries shared by all conceptual designs are shown in Figure 4.1. We have also adopted the Eurocode recommended partial factor γ_{M1} for structural analyses, with its value specified at 1.10 for bridge members. Furthermore, to ensure the safety of the bridge's structural elements, we chose to stay within the elastic field, considering the highest load and the lowest elastic section modulus W_{el} . This modulus is utilized to determine the bending moment resistance, as explained in Section 2.5. Concerning imperfections, we chose to adopt the buckling curve c specified in Section 2.6 and shown in Figure 2.8, with an imperfection factor α set at 0.49.

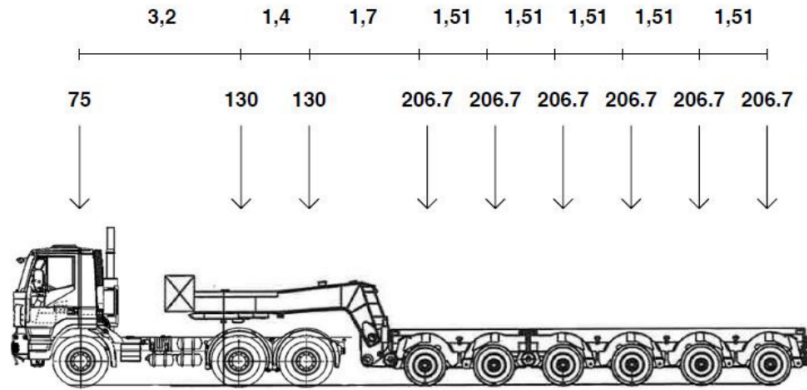
Regarding instability, given the low bending moments determined in both the x and y directions for arch cross-sections, the Equation 2.15 in Section 2.6, *Stability of Tied-Arch bridges*, was simplified by neglecting the bending moment terms. Therefore, the buckling analyses were computed by satisfying:

$$\frac{N_{Ed} \cdot \gamma_{M1}}{\chi \cdot f_{yk} \cdot A} \leq 1 \quad (4.1)$$

Moreover, for in-plane buckling, Figure 2.11 illustrates the determination of the buckling factor β . By considering our bridge with a deck length of 65 meters and a p value of 3.60 meters (*i.e.*, the distance between the hangers), we find that the corresponding value of m is 17. The closest curve value is associated to m equal to 11, to which we will consistently refer when calculating the in-plane buckling factor β . About the out-of-plane buckling instead, we simplified the process by assuming the buckling factor β_2 to be 0.65 for each conceptual design (thus, the total load q and the load part transmitted by hangers q_H are set equal to each other). Finally, as

Table 4.2: *Non-structural dead loads, including their values and units.*

Non-Structural Dead Load	Value	Unit
Pavement	34.10	kN/m
Lateral ledge	15.10	kN/m
Sidings	2.40	kN/m
Guard rails	3.00	kN/m
Plexiglass protections	2.00	kN/m
Central ledge	12.00	kN/m
Protective barriers for hangers	3.00	kN/m

**Figure 4.2:** *Oversize transient load applied across the deck of the bridge. Distances are expressed in meters and the forces in kN.*

explained in Subsection 3.4.2, non-structural elements must be defined. Table 4.2 lists all non-structural elements that were considered for the total non-structural dead load of the bridge and their load values.

Another common aspect across the conceptual designs, in addition to non-structural dead loads, is an oversized transient load that was applied across the deck of the bridge. In our modeling, we considered a 13.85 meters long truck having nine-axle load groups, disposed as shown in Figure 4.2, similarly to what studied by Cantelmi *et al.* in [47]. Starting with the axle of the driving wheels, we applied a force of 75 kN for the first axle, 130 kN for the second and third axles, and 206.7 kN for the remaining axles. In Strand7[®], in order to model the transient load, we defined a vehicle velocity of 30 km/h with a single lane instance. Furthermore, we established four response variables: a shear force response variable for the abutment, another axial response variable assigned to the apex of the arch, and axial and bending moment response variables were instead set to the middle of the deck.

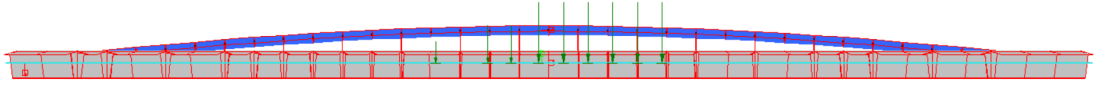


Figure 4.3: *Finite element model for conceptual design 1, having a rise-to-span ratio of 0.03.*

4.2.2 Conceptual Design 1: A Rise-to-Span Ratio of 0.03

The first proposed conceptual design has an f/l ratio of 0.03 ($CD_{f/l=0.03}$), resulting in a bridge with a 2 meters high arch, as shown in Figure 4.3. For this conceptual design, meeting the criteria for snap-through analysis becomes challenging when opting for the double non-articulated arch configuration, known for its heightened safety, due to the relatively low maximum height of the arch compared to the length of the deck. In fact, with an f/l ratio of 0.03, the table in Figure 2.13 reveals the highest K value to be 319. Consequently, we went for the double-articulated arch configuration, sacrificing some safety but ensuring positive snap-through instability checks with a K value of 35. To offset this choice, we maintained a higher cross-sectional area for the arch at 0.169 square meters. Furthermore, the geometry-dependent variables were automatically defined as explained in Subsection 3.2.2.

Despite the increased area, the buckling load multiplier triggering the initial form of global instability (α_{cr}) did not exceed the Eurocode's recommended value of 10 for a global first-order analysis, as described in Subsection 2.6.3. Consequently, we conducted a second-order analysis, adopting the deformed configuration of the arch. Given that the length of the deck exceeds 20 meters, we chose to implement an out-of-plane imperfection with an eccentricity e_0 equal to:

$$e_0 = \frac{\sqrt{20 \cdot l}}{200} = 0.1803 \text{ m} \quad (4.2)$$

Hence, we performed an arch shape parametrization for the finite element model involving this eccentricity as explained in Subsection 3.3.2. Subsequently, a specific oversize load was applied for the influence line study. Thus, the four response variables were defined, and the load influence is then conducted, followed by the linear static and linear buckling analyses. This leads to the identification of stresses acting on the bridge and the critical buckling load multiplier. This information is essential to determine whether a first or second-order global analysis is required, as explained in Subsection 2.6.3. The load positions that maximize the shear stress in the abutment, the compressive stress at the apex of the arch, and the tension stress and bending moment in the middle of the deck are provided. Moreover, we conducted in-plane and out-of-plane buckling analyses. For in-plane buckling, Figure 2.11 shows that the f/l ratio of 0.03 for the curve with m equal to 11 identifies a buckling factor β of 0.28. Hence, the simplified Equation 4.1 was satisfied as follows:

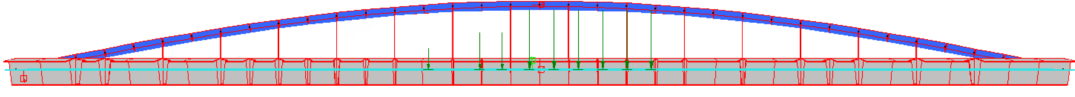


Figure 4.4: *Finite element model for conceptual design 2, having a rise-to-span ratio of 0.06.*

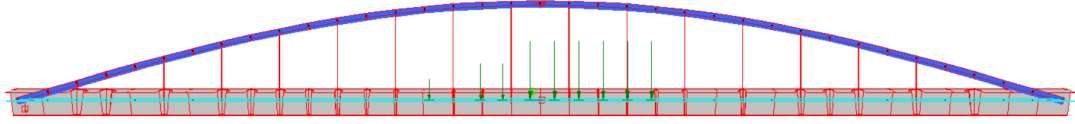


Figure 4.5: *Finite element model for conceptual design 3, having a rise-to-span ratio of 0.09.*

$$\frac{N_{Ed} \cdot \gamma_{M1}}{\chi \cdot f_{yk} \cdot A} = 0.56 \leq 1 \rightarrow \textbf{Positive check}$$

For out-of-plane buckling instead, the value of β_1 listed in Figure 2.14 for an f/l ratio of 0.03 and a constant moment of inertia is set equal to 0.50, while β_2 is always set equal to 0.65. Therefore, the simplified Equation 4.1 was satisfied as follows:

$$\frac{N_{Ed} \cdot \gamma_{M1}}{\chi \cdot f_{yk} \cdot A} = 0.54 \leq 1 \rightarrow \textbf{Positive check}$$

The final step of the optimization process involves Python, where snap-through and resistance analyses are conducted and, finally, the objective function score is calculated. The geometries, parameters, stresses and final objective function scores are all summarized in Table 4.3.

4.2.3 Conceptual Design 2: A Rise-to-Span Ratio of 0.06

The second proposed conceptual design has an f/l ratio of 0.06 ($CD_{f/l=0.06}$), resulting in a bridge with a 4 meters high arch, as depicted in Figure 4.4. For this conceptual design, the optimization process and checks follow a procedure similar to the one specified for the previous conceptual design, *i.e.* $CD_{f/l=0.03}$. Thus, we conducted a second-order analysis and considered a double-articulated arch configuration for snap-through analysis. The geometries, parameters, stresses and final objective function scores are all summarized in Table 4.4.

4.2.4 Conceptual Design 3: A Rise-to-Span Ratio of 0.09

The third proposed conceptual design has an f/l ratio of 0.09 ($CD_{f/l=0.09}$), which yields a bridge with a 6 meters high arch, as illustrated in Figure 4.5. For the snap-through analysis of $CD_{f/l=0.09}$, we decided to adopt a more safety non-articulated

4. Results and Discussion

Table 4.3: Geometries, parameters, stresses and final objective function results for conceptual design 1, having a rise-to-span ratio of 0.03.

Arch cross-section's plate	Thickness (m)	Length (m)	Area (m ²)
Plate A ×2	0.05	0.25	0.013
Plate B ×2	0.04	0.72	0.029
Plate C ×1	0.04	0.46	0.018
Plate D ×1	0.05	1.40	0.070
Total approximate area			0.169
Parameter	Acronym	Value	Unit
Moment of inertia about the x -axis	I_x	5.13×10^{-3}	m ⁴
Moment of inertia about the y -axis	I_y	3.21×10^{-2}	m ⁴
Angle from the center of the arch	θ	14	°
Radius	r	267.95	m
Circumference	C	1683.58	m
Arch length	S	65.16	m
Critical buckling load multiplier	α_{cr}	8.07	
Half arch length	s	32.56	m
Critical in-plane buckling load	C_{cr}	127 846	kN
Snap-through factor	K	35	
In-plane buckling factor	β	0.28	
In-plane factor	$\tilde{\lambda}$	0.69	
In-plane factor	Φ	0.85	
In-plane factor	χ	0.73	
Critical out-of-plane buckling load	C_{cr}	148 746	kN
Out-of-plane buckling factor	β_1	0.50	
Out-of-plane buckling factor	β_2	0.65	
Out-of-plane factor	$\tilde{\lambda}$	0.64	
Out-of-plane factor	Φ	0.81	
Out-of-plane factor	χ	0.76	
Stress	Load position	Value	Unit
Arch apex max compression	Middle deck	22 458	kN
Abutment max shear force	Middle deck	2743	kN
Middle deck max tension	Middle deck	22 348	kN
Middle deck max bending moment	Middle deck	46 540	kNm
Resistance analysis		Comparison	Check
Arch compression		$22\,458 < 54\,541$	Positive check
Abutment shear force		$2743 < 115\,150$	Positive check
Deck tension		$22\,348 < 199\,445$	Positive check
Deck bending moment		$46\,540 < 211\,709$	Positive check
Objective function result		Value	Unit
Steel weight		86 445	kg
Cost		62 240	€
CO ₂ emitted		176 694	kg

Table 4.4: Geometries, parameters, stresses and final objective function results for conceptual design 2, having a rise-to-span ratio of 0.06.

Arch cross-section's plate	Thickness (m)	Length (m)	Area (m ²)
Plate A ×2	0.05	0.25	0.013
Plate B ×2	0.04	0.65	0.026
Plate C ×1	0.04	0.46	0.018
Plate D ×1	0.05	1.30	0.065
Total approximate area			0.161
Parameter	Acronym	Value	Unit
Moment of inertia about the x -axis	I_x	4.82×10^{-3}	m ⁴
Moment of inertia about the y -axis	I_y	2.65×10^{-2}	m ⁴
Angle from the center of the arch	θ	28	°
Radius	r	134.97	m
Circumference	C	848.05	m
Arch length	S	65.65	m
Critical buckling load multiplier	α_{cr}	8.53	
Half arch length	s	32.83	m
Critical in-plane buckling load	C_{cr}	110 363	kN
Snap-through factor	K	35	
In-plane buckling factor	β	0.29	
In-plane factor	$\tilde{\lambda}$	0.72	
In-plane factor	Φ	0.87	
In-plane factor	χ	0.71	
Critical out-of-plane buckling load	C_{cr}	122 780	kN
Out-of-plane buckling factor	β_1	0.50	
Out-of-plane buckling factor	β_2	0.65	
Out-of-plane factor	$\tilde{\lambda}$	0.68	
Out-of-plane factor	Φ	0.85	
Out-of-plane factor	χ	0.74	
Stress	Load position	Value	Unit
Arch apex max compression	Middle deck	18 140	kN
Abutment max shear force	Deck edge	2562	kN
Middle deck max tension	Middle deck	17 810	kN
Middle deck max bending moment	Middle deck	20 373	kNm
Resistance analysis		Comparison	Check
Arch compression		$18\,140 < 51\,959$	Positive check
Abutment shear force		$2562 < 115\,150$	Positive check
Deck tension		$17\,810 < 199\,445$	Positive check
Deck bending moment		$20\,373 < 211\,709$	Positive check
Objective function result		Value	Unit
Steel weight		82 966	kg
Cost		59 735	€
CO ₂ emitted		169 582	kg

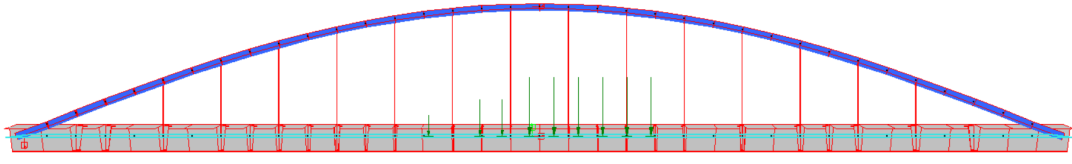


Figure 4.6: *Finite element model for conceptual design 4, having a rise-to-span ratio of 0.12.*

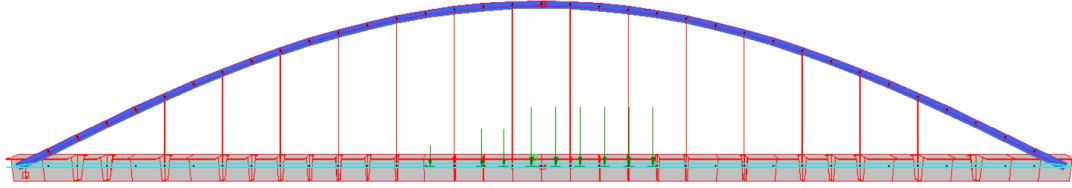


Figure 4.7: *Finite element model for conceptual design 5, having a rise-to-span ratio of 0.15.*

arch configuration, with a K value of 42. On top of that, we saw that the buckling load multiplier α_{cr} for $CD_{f/l=0.09}$ is greater than 10, meaning that a second-order analysis was not required. The rest of the optimization process is again similar to the previous conceptual designs, *i.e.*, $CD_{f/l=0.03}$ and $CD_{f/l=0.06}$. Its geometries, parameters, stresses and final objective function scores are all summarized in Table 4.5.

4.2.5 Conceptual Design 4: A Rise-to-Span Ratio of 0.12

Figure 4.6 shows our fourth conceptual design, defined with a f/l ratio of 0.12 ($CD_{f/l=0.12}$). The resulting bridge is characterized by an 8 meters high arch. For optimizing $CD_{f/l=0.12}$, we followed the same steps performed for design $CD_{f/l=0.09}$. Geometries, parameters, stresses and final objective function scores are all summarized in Table 4.6.

4.2.6 Conceptual Design 5: A Rise-to-Span Ratio of 0.15

For the fifth and last proposed conceptual design, we fixed the f/l ratio to 0.15 ($CD_{f/l=0.15}$), that is, a bridge with a 10 meters high arch, as shown in Figure 4.7. Design $CD_{f/l=0.15}$ optimization process and check align with the ones performed for $CD_{f/l=0.09}$ and $CD_{f/l=0.12}$. The final objective function scores, geometries, parameters, and stresses are summarized in Table 4.7.

Table 4.5: Geometries, parameters, stresses and final objective function results for conceptual design 3, having a rise-to-span ratio of 0.09.

Arch cross-section's plate	Thickness (m)	Length (m)	Area (m ²)
Plate A ×2	0.05	0.21	0.011
Plate B ×2	0.04	0.68	0.027
Plate C ×1	0.04	0.40	0.016
Plate D ×1	0.05	1.32	0.066
Total approximate area			0.153
Parameter	Acronym	Value	Unit
Moment of inertia about the x -axis	I_x	3.66×10^{-3}	m ⁴
Moment of inertia about the y -axis	I_y	2.14×10^{-2}	m ⁴
Angle from the center of the arch	θ	42	°
Radius	r	91.10	m
Circumference	C	572.42	m
Arch length	S	66.46	m
Critical buckling load multiplier	α_{cr}	10.03	
Half arch length	s	33.23	m
Critical in-plane buckling load	C_{cr}	69 130	kN
Snap-through factor	K	42	
In-plane buckling factor	β	0.30	
In-plane factor	$\tilde{\lambda}$	0.89	
In-plane factor	Φ	1.06	
In-plane factor	χ	0.61	
Critical out-of-plane buckling load	C_{cr}	100 344	kN
Out-of-plane buckling factor	β_1	0.54	
Out-of-plane buckling factor	β_2	0.65	
Out-of-plane factor	$\tilde{\lambda}$	0.74	
Out-of-plane factor	Φ	0.90	
Out-of-plane factor	χ	0.70	
Stress	Load position	Value	Unit
Arch apex max compression	Middle deck	13 880	kN
Abutment max shear force	Deck edge	2214	kN
Middle deck max tension	Middle deck	13 338	kN
Middle deck max bending moment	Deck edge	14 466	kNm
Resistance analysis		Comparison	Check
Arch compression		$13\,880 < 49\,377$	Positive check
Abutment shear force		$2214 < 115\,150$	Positive check
Deck tension		$13\,338 < 199\,445$	Positive check
Deck bending moment		$14\,466 < 211\,709$	Positive check
Objective function result		Value	Unit
Steel weight		79 827	kg
Cost		57 475	€
CO ₂ emitted		163 166	kg

Table 4.6: Geometries, parameters, stresses and final objective function results for conceptual design 4, having a rise-to-span ratio of 0.12.

Arch cross-section's plate	Thickness (m)	Length (m)	Area (m ²)
Plate A ×2	0.05	0.20	0.010
Plate B ×2	0.05	0.62	0.031
Plate C ×1	0.04	0.40	0.016
Plate D ×1	0.05	1.20	0.060
Total approximate area			0.156
Parameter	Acronym	Value	Unit
Moment of inertia about the x -axis	I_x	3.66×10^{-3}	m ⁴
Moment of inertia about the y -axis	I_y	2.14×10^{-2}	m ⁴
Angle from the center of the arch	θ	56	°
Radius	r	69.53	m
Circumference	C	436.88	m
Arch length	S	67.64	m
Critical buckling load multiplier	α_{cr}	10.08	
Half arch length	s	33.82	m
Critical in-plane buckling load	C_{cr}	60 913	kN
Snap-through factor	K	42	
In-plane buckling factor	β	0.33	
In-plane factor	$\tilde{\lambda}$	0.95	
In-plane factor	Φ	1.14	
In-plane factor	χ	0.57	
Critical out-of-plane buckling load	C_{cr}	85 149	kN
Out-of-plane buckling factor	β_1	0.54	
Out-of-plane buckling factor	β_2	0.65	
Out-of-plane factor	$\tilde{\lambda}$	0.81	
Out-of-plane factor	Φ	0.97	
Out-of-plane factor	χ	0.66	
Stress	Load position	Value	Unit
Arch apex max compression	Middle deck	11 273	kN
Abutment max shear force	Deck edge	2063	kN
Middle deck max tension	Middle deck	10 525	kN
Middle deck max bending moment	Deck edge	12 033	kNm
Resistance analysis		Comparison	Check
Arch compression		$11\,273 < 50\,345$	Positive check
Abutment shear force		$2063 < 115\,150$	Positive check
Deck tension		$10\,525 < 199\,445$	Positive check
Deck bending moment		$12\,033 < 211\,709$	Positive check
Objective function result		Value	Unit
Steel weight		82 826	kg
Cost		59 635	€
CO ₂ emitted		169 296	kg

Table 4.7: Geometries, parameters, stresses and final objective function results for conceptual design 5, having a rise-to-span ratio of 0.15.

Arch cross-section's plate	Thickness (m)	Length (m)	Area (m ²)
Plate A ×2	0.05	0.22	0.011
Plate B ×2	0.05	0.57	0.029
Plate C ×1	0.05	0.43	0.022
Plate D ×1	0.05	1.10	0.055
Total approximate area			0.156
Parameter	Acronym	Value	Unit
Moment of inertia about the x -axis	I_x	3.89×10 ⁻³	m ⁴
Moment of inertia about the y -axis	I_y	1.94×10 ⁻²	m ⁴
Angle from the center of the arch	θ	70	°
Radius	r	56.90	m
Circumference	C	357.51	m
Arch length	S	69.18	m
Critical buckling load multiplier	α_{cr}	10.06	
Half arch length	s	34.59	m
Critical in-plane buckling load	C_{cr}	42 062	kN
Snap-through factor	K	13	
In-plane Buckling factor	β	0.40	
In-plane factor	$\tilde{\lambda}$	1.15	
In-plane factor	Φ	1.39	
In-plane factor	χ	0.46	
Critical out-of-plane buckling load	C_{cr}	77 171	kN
Out-of-plane Buckling factor	β_1	0.54	
Out-of-plane Buckling factor	β_2	0.65	
Out-of-plane factor	$\tilde{\lambda}$	0.85	
Out-of-plane factor	Φ	1.02	
Out-of-plane factor	χ	0.63	
Stress	Load position	Value	Unit
Arch apex max compression	Middle deck	9547	kN
Abutment max shear force	Deck edge	1996	kN
Middle deck max tension	Middle deck	8609	kN
Middle deck max bending moment	Deck edge	11 253	kNm
Resistance analysis		Comparison	Check
Arch compression		9547 kN < 50 345 kN	Positive check
Abutment shear force		1996 kN < 115 150 kN	Positive check
Deck tension		8609 kN < 199 445 kN	Positive check
Deck bending moment		11 253 kNm < 211 709 kNm	Positive check
Objective function result		Value	Unit
Steel weight		84 722	kg
Cost		61 000	€
CO ₂ emitted		173 173	kg

4.3 Discussion

In our analysis of various design modifications for the tied-arch bridge, we identified significant trends and differences in terms of their structural efficiency and environmental impact. This discussion integrates the detailed results presented in Table 4.9 and the graphical representation in Figure 4.8, which elucidate the savings in steel weight, cost, and CO₂ emissions compared to the original bridge design and they are listed as follows:

- The design variant $CD_{f/l=0.03}$ was characterized by its low f/l ratio, diverging significantly from conventional design norms. This design was notably less efficient, as evidenced by an increased requirement for steel compared to the baseline model. The objective function results indicated a negative outcome for this design variant, underscoring its impracticality;
- the design variant $CD_{f/l=0.09}$ stood out as the most efficient and environmentally friendly option. It achieved a remarkable reduction in steel usage, leading to lowered construction costs and a 6.80 % decrease in CO₂ emissions, as detailed in Table 4.9 and Figure 4.8;
- the design variant $CD_{f/l=0.15}$ exhibited the least improvement in environmental impact. The design yielded only a marginal reduction of 1.09 % in steel usage, cost, and CO₂ emissions compared to the original design. This result suggests a cutoff point in design optimization for bridges of this specific type and length, indicating that further increases in arch height beyond this point may produce diminishing returns.

In conclusion, our analysis reaffirms the feasibility of optimizing the bridge design for enhanced sustainability. The varied efficacy of different design variations, as highlighted in Figure 4.8 and Table 4.9, illustrates the delicate balance between structural requirements and environmental sustainability. While the study confirms that improvements are possible and beneficial, it also respects the high quality of the original design.

Table 4.8: Arch cross-sectional area (A_a) and objective function results (steel weight $W_{tot,a}$, cost $C_{tot,a}$ and carbon dioxide emitted $CO_{2eqe,a}$) for both the reference design (R.D) and each conceptual design studied (C.D).

Design	f/l	A_a (m ²)	$W_{tot,a}$ (kg)	$C_{tot,a}$ (€)	$CO_{2eqe,a}$ (kg)
$RD_{f/l=0.10}$	0.10	0.163	85 654	61 671	175 076
$CD_{f/l=0.03}$	0.03	0.169	86 445	62 240	176 694
$CD_{f/l=0.06}$	0.06	0.161	82 966	59 735	169 582
$CD_{f/l=0.09}$	0.09	0.153	79 827	57 475	163 166
$CD_{f/l=0.12}$	0.12	0.156	82 826	59 635	169 296
$CD_{f/l=0.15}$	0.15	0.156	84 722	61 000	173 173

Table 4.9: Objective function scores (steel weight W_{score} , cost C_{score} and carbon dioxide emitted $CO_{2eqe,score}$) calculated for each conceptual design, along with their percentage difference compared to the original design.

Design	f/l	A_a (m ²)	W_{score} (kg)	C_{score} (€)	$CO_{2eqe,score}$ (kg)	Difference
$CD_{f/l=0.03}$	0.03	0.169	791	569	1618	-0.92 % Spending
$CD_{f/l=0.06}$	0.06	0.161	2688	1936	5494	+3.14 % Saving
$CD_{f/l=0.09}$	0.09	0.153	5827	4196	11 910	+6.80 % Saving
$CD_{f/l=0.12}$	0.12	0.156	2828	2036	5780	+3.30 % Saving
$CD_{f/l=0.15}$	0.15	0.156	932	671	1903	+1.09 % Saving

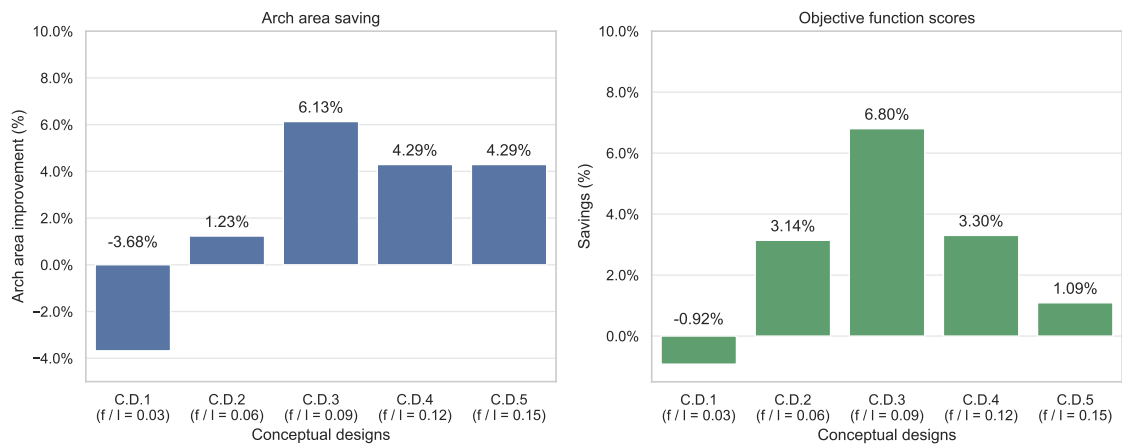


Figure 4.8: Arch area saving and the objective function scores percentage for each conceptual design (C.D.) compared to the original design.

5

Conclusion

This thesis has presented an innovative optimization process tailored for assessing and optimizing the environmental impact of tied-arch bridges. Central to this process was the calculation of steel quantities used in construction, alongside associated costs and CO₂ emissions. Focusing on the arch's shape and cross-sectional geometries, a real-life existing bridge was analyzed and compared against alternative designs with varied arch configurations. Notably, one of these alternatives achieved a significant maximum saving of 6.80 % compared to the original design. This result not only underscores the high quality of the original design but also validates the feasibility and potential for meaningful optimization in similar case studies.

5.1 Future Work

The algorithm developed in this research has demonstrated its capability for conducting case studies and numerical experiments. However, for it to be applicable in real-world design scenarios, further development and validation are necessary. This section outlines potential avenues for extending this research.

5.1.1 API Implementation

The integration of Strand7[®] API with Python, as described by Meng *et al.* [48], offers an exciting prospect for enhancing our algorithm. This approach allows for direct communication between the finite element analysis software and Python, facilitating automated updates of design variables and extraction of structural analysis results. Utilizing this API can streamline the process of resistance verification and objective function calculation, thereby improving the software's practicality and efficiency in structural design.

5.1.2 SciPy Optimization in Python

Python's robust ecosystem, particularly the SciPy library [49], presents a promising direction for advancing computational optimization methodologies. Despite differences from the manual optimization approach used in this thesis, the fundamental steps of defining variables, constants, and objective functions remain consistent. The application of SciPy's optimization algorithms can significantly expedite the optimization process, although challenges in accurately defining the objective function

and constraints for complex designs like tied-arch bridges should be acknowledged and addressed.

5.1.3 Increase Level of Design Detail

Enhancing the study to include a variety of structural steel types, as opposed to solely using steel grade S355, could provide deeper insights into the environmental and structural impacts of material choices. Expanding the scope to encompass additional structural components and conducting more comprehensive structural analyses, such as fatigue assessments [40], would contribute to a more holistic understanding of bridge design and optimization.

5.1.4 Multi Objective Optimization

The research presented has focused on a single objective function to minimize environmental impact. However, real-world engineering challenges often necessitate balancing multiple objectives. Adopting a multi-objective optimization approach, as outlined in Section 2.1, could enable the exploration of trade-offs between various factors, such as construction time and environmental impact. Identifying Pareto solutions in such scenarios would offer a more nuanced understanding of the complexities and trade-offs inherent in bridge design optimization.

Bibliography

- [1] A. E. Long, P. Basheer, S. E. Taylor, B. G. Rankin, and J. Kirkpatrick, "Sustainable bridge construction through innovative advances," in *Proceedings of the Institution of Civil Engineers-Bridge Engineering*, Thomas Telford Ltd, vol. 161, 2008, pp. 183–188.
- [2] L. Mei and Q. Wang, "Structural optimization in civil engineering: A literature review," *Buildings*, vol. 11, no. 2, p. 66, 2021.
- [3] N. J. Santero and A. Horvath, "Global warming potential of pavements," *Environmental Research Letters*, vol. 4, no. 3, p. 034011, 2009.
- [4] O. Skoglund, J. Leander, and R. Karoumi, "Optimizing the steel girders in a high strength steel composite bridge," *Engineering Structures*, vol. 221, p. 110981, 2020.
- [5] S. El Mourabit, *Optimization of concrete beam bridges: Development of software for design automation and cost optimization*, 2016.
- [6] S. P. Rajput and S. Datta, "A review on optimization techniques used in civil engineering material and structure design," *Materials Today: Proceedings*, vol. 26, pp. 1482–1491, 2020.
- [7] K. Korus, M. Salamak, and M. Jasiński, "Optimization of geometric parameters of arch bridges using visual programming fem components and genetic algorithm," *Engineering Structures*, vol. 241, p. 112465, 2021.
- [8] A. Kaveh and S. Talatahari, "A novel heuristic optimization method: Charged system search," *Acta mechanica*, vol. 213, no. 3-4, pp. 267–289, 2010.
- [9] D. E. Kvasov and M. S. Mukhametzhanov, "Metaheuristic vs. deterministic global optimization algorithms: The univariate case," *Applied Mathematics and Computation*, vol. 318, pp. 245–259, 2018.
- [10] A. Kaveh and M. Khayatazad, "A new meta-heuristic method: Ray optimization," *Computers & structures*, vol. 112, pp. 283–294, 2012.
- [11] A. Khedr, B. Tolson, and S. Ziemann, "Water distribution system calibration: Manual versus optimization-based approach," *Procedia Engineering*, vol. 119, pp. 725–733, 2015.
- [12] D. A. Van Veldhuizen, G. B. Lamont, *et al.*, "Evolutionary computation and convergence to a pareto front," in *Late breaking papers at the genetic programming 1998 conference*, Citeseer, 1998, pp. 221–228.
- [13] J. A. Joines and C. R. Houck, "On the use of non-stationary penalty functions to solve nonlinear constrained optimization problems with ga's," in *Proceedings of the first IEEE conference on evolutionary computation. IEEE world congress on computational intelligence*, IEEE, 1994, pp. 579–584.

- [14] M. H. Afshar, A. Afshar, M. Marino, *et al.*, “An iterative penalty method for the optimal design of pipe networks,” 2009.
- [15] J. B. Rosen, “The gradient projection method for nonlinear programming. part i. linear constraints,” *Journal of the society for industrial and applied mathematics*, vol. 8, no. 1, pp. 181–217, 1960.
- [16] P. E. Gill, W. Murray, M. A. Saunders, and M. H. Wright, “Procedures for optimization problems with a mixture of bounds and general linear constraints,” *ACM Transactions on Mathematical Software (TOMS)*, vol. 10, no. 3, pp. 282–298, 1984.
- [17] K. Krabbenhoft and L. Damkilde, “A general non-linear optimization algorithm for lower bound limit analysis,” *International Journal for Numerical Methods in Engineering*, vol. 56, no. 2, pp. 165–184, 2003.
- [18] A. B. Solanki, J. R. Parikh, and R. H. Parikh, “Formulation and optimization of piroxicam proniosomes by 3-factor, 3-level box-behnken design,” *Aaps Pharmscitech*, vol. 8, pp. 43–49, 2007.
- [19] X. Du, “Reliability-based design optimization with dependent interval variables,” *International Journal for Numerical Methods in Engineering*, vol. 91, no. 2, pp. 218–228, 2012.
- [20] S. Sundaresan, K. Ishii, and D. R. Houser, “A robust optimization procedure with variations on design variables and constraints,” *Engineering Optimization+ A35*, vol. 24, no. 2, pp. 101–117, 1995.
- [21] H. De Backer, A. Outtier, and P. Van Bogaert, “Buckling design of steel tied-arch bridges,” *Journal of Constructional Steel Research*, vol. 103, pp. 159–167, 2014.
- [22] P. Lonetti, A. Pascuzzo, and S. Aiello, “Instability design analysis in tied-arch bridges,” *Mechanics of Advanced materials and Structures*, vol. 26, no. 8, pp. 716–726, 2019.
- [23] M. Vlad, G. Kollo, and V. Marusceac, “A modern approach to tied-arch bridge analysis and design,” *Acta Technica Corviniensis-Bulletin of Engineering*, vol. 8, no. 4, p. 33, 2015.
- [24] K. M. Sennah and J. B. Kennedy, “Literature review in analysis of box-girder bridges,” *Journal of Bridge Engineering*, vol. 7, no. 2, pp. 134–143, 2002.
- [25] K. M. Sennah and J. B. Kennedy, “State-of-the-art in design of curved box-girder bridges,” *Journal of Bridge Engineering*, vol. 6, no. 3, pp. 159–167, 2001.
- [26] Y. Zeinali and B. A. Story, “Impairment localization and quantification using noisy static deformation influence lines and iterative multi-parameter tikhonov regularization,” *Mechanical Systems and Signal Processing*, vol. 109, pp. 399–419, 2018.
- [27] A. Martini, E. M. Tronci, M. Q. Feng, and R. Y. Leung, “A computer vision-based method for bridge model updating using displacement influence lines,” *Engineering Structures*, vol. 259, p. 114129, 2022.
- [28] Y. Zeinali and B. A. Story, “Framework for flexural rigidity estimation in euler-bernoulli beams using deformation influence lines,” *Infrastructures*, vol. 2, no. 4, p. 23, 2017.

-
- [29] *Suspension bridge*, https://en.wikipedia.org/wiki/Suspension_bridge, last edit on 16 November 2023.
 - [30] *Arch bridge*, https://en.wikipedia.org/wiki/Arch_bridge, last edit on 15 August 2023.
 - [31] *Tied-arch bridge*, https://en.wikipedia.org/wiki/Tied-arch_bridge, last edit on 15 August 2023.
 - [32] P. Lonetti, A. Pascuzzo, A. Davanzo, *et al.*, “Dynamic behavior of tied-arch bridges under the action of moving loads,” *Mathematical Problems in Engineering*, vol. 2016, 2016.
 - [33] A. P. de Construção *et al.*, *Design of Steel Structures: Eurocode 3: Design of Steel Structures, Part 1-1: General Rules and Rules for Buildings*. John Wiley & Sons, 2016.
 - [34] J. K. Paik and A. K. Thayamballi, *Ultimate limit state design of steel-plated structures*. John Wiley & Sons, 2003.
 - [35] B. En, “2, eurocode 3: Design of steel structures: Part 2: Steel bridges,” *British Standards Institution*, 2006.
 - [36] R. T. Haftka, R. H. Mallett, *et al.*, “Adaption of koiter’s method to finite element analysis of snap-through buckling behavior,” *International Journal of Solids and Structures*, vol. 7, no. 10, pp. 1427–1445, 1971.
 - [37] J.-W. Lin, R. Betti, A. W. Smyth, and R. W. Longman, “On-line identification of non-linear hysteretic structural systems using a variable trace approach,” *Earthquake engineering & structural dynamics*, vol. 30, no. 9, pp. 1279–1303, 2001.
 - [38] O. A. Bauchau and J. I. Craig, “Euler-bernoulli beam theory,” in *Structural analysis*, Springer, 2009, pp. 173–221.
 - [39] G. Bongiovanni, F. Luccio, and A. Zorat, “The discrete equation of the straight line,” *IEEE Transactions on Computers*, vol. 100, no. 3, pp. 310–313, 1975.
 - [40] C. Pellegrino, G. Cupani, and C. Modena, “The effect of fatigue on the arrangement of hangers in tied arch bridges,” *Engineering Structures*, vol. 32, no. 4, pp. 1140–1147, 2010.
 - [41] A. Palermo, F. Sarti, A. Baird, D. Bonardi, D. Dekker, and S. Chung, “From theory to practice: Design, analysis and construction of dissipative timber rocking post-tensioning wall system for carterton events centre, new zealand,” in *Proceedings of the 15th World Conference on earthquake engineering, Lisbon, Portugal*, 2012, pp. 24–28.
 - [42] R. Nelson and D. Lorch, “A refined theory for laminated orthotropic plates,” 1974.
 - [43] J. Doležel, D. Novák, and J. Petr, “Assessment of the transportation route of oversize and excessive loads in relation to the load-bearing capacity of existing bridges,” in *IOP Conference Series: Materials Science and Engineering*, IOP Publishing, vol. 236, 2017, p. 012070.
 - [44] *Load infl.* <https://www.strand7.com/html/movingload/LoadInfluences.htm>, Strand7 Release 3.1.3 (R3.1.3).
 - [45] *Strand7 l.s. solver*, <https://www.strand7.com/html/linearstatic.ht>, Strand7 Release 3.1.3 (R3.1.3).

- [46] *Strand7 l.b. solver*, <https://www.strand7.com/html/linearbuckling.htm>, Strand7 Release 3.1.3 (R3.1.3).
- [47] D. Cantelmi, “Effetto dei carichi eccezionali su strutture da ponte= transit of exceptional vehicles: Effects on bridges,” Ph.D. dissertation, Politecnico di Torino, 2020.
- [48] M. Meng, S. Steinhardt, and A. Schubert, “Application programming interface documentation: What do software developers want?” *Journal of Technical Writing and Communication*, vol. 48, no. 3, pp. 295–330, 2018.
- [49] P. Virtanen, R. Gommers, T. E. Oliphant, *et al.*, “Scipy 1.0: Fundamental algorithms for scientific computing in python,” *Nature methods*, vol. 17, no. 3, pp. 261–272, 2020.